VIBRATION ANALYSIS OF BCC LATTICE STRUCTURE MATERIALS USING FINITE ELEMENT METHOD

MUHAMMAD NASRUDDIN BIN NURDIN

UNIVERSITI TEKNIKAL MALAYSIA MELAKA

VIBRATION ANALYSIS OF BCC LATTICE STRUCTURE MATERIALS USING FINITE ELEMENT METHOD

MUHAMMAD NASRUDDIN BIN NURDIN

This report is submitted
in fulfillment of the requirement for the degree of
Bachelor of Mechanical Engineering

Faculty of Mechanical Engineering

UNIVERSITI TEKNIKAL MALAYSIA MELAKA

MAY 2019

STUDENT DECLARATION

I declare that this project report entitled "Vibration analysis of BCC Lattice Structure Material Using Finite Element Method" is the result of my own work except as cited in the references

Signature	:	....
Name	:	Muhammad Nasruddin Bin Nurdin
Date	:	....

SUPERVISOR'S APPROVAL

I have checked this report and the report can now be submitted to JK-PSM to be delivered back to supervisor and to the second examiner.

Signature	:	....
Name	:	Dr. Rainah Binti Ismail
Date	:	....

DEDICATION

To Allah s.w.t, Alhamdulillah for your blessing.

To my beloved mother and father.

Thank you for your love, support and understand.

May Allah grant us a forever Jannah.

To supervisor,

Thank you for your knowledge, guidance, patience and support.

May Allah grant you goodness and blessings.

ABSTRACT

Lattice structure has increasing interest amongst researchers due to its vast advantages features such as lightweight properties, high mechanical strength and high energy absorbance. In this report, the effect of strut diameter design parameter of quatrefoil shaped BCC lattice structure on its natural frequency is investigated. The quatrefoil shape BCC lattice structure bar sample with different strut diameter sizes were made by using the fused deposition modelling (FDM) additive manufacturing (AM) technique. The bar sample were subjected to vibration testing with set up consist of fabricated test rig, accelerometer, impact hammer and signal generator/analyzer. Likewise, FEM models using ABAQUS software are also constructed to investigate their natural frequency and deformation numerically. From the vibration testing, the sample with highest strut diameter produced highest natural frequency value due to increased stiffness. It is found that the numerical results are in good agreement with less than 17% error with the experimental results. Using the experimentally validated FEM model the effect of strut diameter to the stiffness of lattice structure are further investigated to support the findings in vibration testing. The stiffness obtained shows similar increasing trend like that of in the vibration testing as the strut diameter size increase. The conclusion that can derived from this study are the size of strut diameter are affected the natural frequency also the stiffness of lattice structure bar sample. Therefore, the information of lattice structure in this study are shows that lattice structure is suitable use in dynamic application.

ABSTRAK

Struktur berbentuk kekisi telah meningkatkan minat para penyelidik kerana kelebihannya yang luas seperti sifat ringan, kekuatan mekanikal yang tinggi dan penyerapan tenaga yang tinggi. Dalam laporan ini, kesan parameter reka bentuk ukur lilit jejari struktur kekisi BCC berbentuk 'Quatrefoil' pada frekuensi semula jadi telah disiasat. Bentuk 'Quatrefoil' BCC struktur kekisi dengan saiz jejari yang berbeza dihasilkan dengan menggunakan 'Fused Deposition Modelling' (FDM) kaedah pembuatan secara tambahan. Sampel bar tertakluk kepada ujian getaran yang disediakan terdiri daripada rig ujian, 'accelerometer', tukul kesan dan penjana isyarat/penganalisis. Begitu juga, model FEM yang menggunakan perisian 'ABAQUS' juga dibina untuk menyiasat frekuensi semula jadi dan ubah bentuk secara berangka. Dari ujian getaran, sampel dengan ukur lilit jejari tertinggi menghasilkan nilai frekuensi semula jadi yang tinggi disebabkan oleh peningkatan kekakuan. Daripada keputusan berangka yang terhasil adalah dalam persetujuan yang baik dengan kurang 17% ralat dengan hasil eksperimen. Selanjutnya, menggunakan model FEM yang disahkan secara eksperimen, kesan ukur lilit jejari kepada kekakuan struktur kekisi akan dikaji selanjutnya untuk menyokong penemuan dalam ujian getaran. Kekakuan yang diperoleh menunjukkan trend peningkatan yang sama seperti dalam ujian getaran kerana saiz ukur lilit jejari meningkat. Kesimpulan yang boleh dibuat dari kajian ini adalah saiz ukur lilit jejari mempengaruhi frekuensi semula jadi juga kekakuan sampel bar struktur kekisi. Oleh itu, maklumat struktur kekisi dalam kajian ini menunjukkan bahawa struktur kekisi sesuai untuk penggunaan dalam aplikasi dinamik.

ACKNOWLEDGEMENT

I would like to express my special thanks of gratitude to my supervisor Dr. Rainah Binti Ismail for giving me this opportunity to do final year project with her. She never hesitated to give me guidance and advice whenever I am having problems. I am thankful for her patience and advice while leading me in this project.

I would also like to extend my gratitude to PhD student named Muhamad Syafwan Azmi for spending his time to guide me. They would share his knowledge in the field of vibration with me and guide me to do experiment. Also, I would like to thank laboratory assistant, En. Jorhadi for his kindness in suggesting me the suitable time to use laboratory equipment for his action saved me a lot of time.

I would like to thank my course mates and postgraduate student for giving me their support, patience and encouragement. Finally, I would like to thank my family for their support.

TABLE OF CONTENTS

LIST OF FIGURES

LIST OF TABLES

LIST OF ABBREAVIATION

ABS	-	Acrylonitrile Butadiene Styrene
AM	-	Additive Manufacturing
BCC	-	Body Centered Cubic
CF	-	Clamped Free
CFRP	-	Carbon Fiber Reinforced Polymer
CM	-	Condition Monitoring
EBM	-	Electron Beam Melting
FDM	-	Fused Deposition Modeling
FEA	-	Finite Element Analysis
GFRP	-	Glass Fiber Reinforced Polymer
MSD	-	Mass Spring Damper
SLA	-	Stereolithography
SLM	-	Selective Laser Melting
SLS	-	Selective Laser Sintering
3D	-	Three Dimension

CHAPTER 1

INTRODUCTION

1.1 Background of Research

Previously, most manufacturers in the automotive and aerospace industries used solid bulk materials to make component which produced heavy body part. As the result, the fuel efficiency is lower besides higher gas emission to the environment. Due to this, nowadays, many manufacturers are shifting materials for lighter body parts or making improvements to the engines or motors. In order to get lighter body parts, this can be done by either using lighter weight materials such as carbon fiber reinforced polymer (CFRP), glass fiber reinforced polymer (GFRP), or using lower density structure such as lattice structures. However, lattice is lightweight materials thus lighter material produce more vibration. Thus, lack of study on the suitability and limitations of this structure can lead to unwanted instances of high vibration. Overtime, vibration effects can have long-term as well as short-term damaging effects on the structure. Such phenomenon's are potentially dangerous as they can create complete unbalance of the structure which can then ultimately fail.

Lattice structure is multi-functional material that can offer good balance of strength, stiffness, cost, durability and relative static and dynamic properties (Ozdemir et al., 2015). The lattice structure material is one of the types of architectured material that can be defined as "a combination of two or more materials, or of material and space, assembled in a way as to have the attributes not offered by any one material alone"(Ashby, 2013). Lattice structure can be used as an alternative for material that has lightweight properties. It can make many advantages for example make lighter aeroplane and thus reduce the uses of fuel for aeroplane (Azman, 2017). There are many types of topological designs of the lattice structure material. The topological designs are based on its elementary of lattice structure or commonly called ‘unit cell’ (Azman, 2017). Example of common lattice structure topological designs are octet-truss, kagome, body centred cubic (BCC) and pyramidal etc.

Lattice structures in nature have been used by human since thousands of years. Before the emerging of additive manufacturing (AM), conventional manufacturing methods such as investment casting (Mun et al., 2015), expanded metal sheet (Kooistra and Wadley, 2007), metallic wire assembly (Queheillalt and Wadley, 2005) and snap fit (Dong et al., 2015) are used to fabricate lattice structure. Nowadays, the use of AM is preferable to fabricate lattice structure materials (Hadi et al., 2015). Examples of previously reported AM methods used to fabricate lattice structure materials are selective laser sintering (SLS), selective laser melting (SLM), stereolithography (SLA), and electron beam melting (EBM) and fused deposition modeling (FDM). Using AM methods allows a significantly higher design complexity of lattice structure to be manufactured as opposed to conventional manufacturing methods due to limitation of the conventional machine (Crupi et al., 2017). Besides that, using AM can saves much time to fabricate lattice structure as it requires shorter process chain.

1.2 Problem Statement

New global progress of regulation regarding fuel efficiency and gas emission of vehicle has led to motivation on weight reduction of vehicle (Abdollah and Hassan, 2013). The development can be made either by using lower weight materials such as CFRP and GFRP composites or using low density structure material such as lattice structure. If the lattice structure is to be used in dynamic applications such as body parts for moving machines and devices due to its lightweight properties that it can be highly beneficial, thus dynamic testing is essential to evaluate the suitability of this structure in such applications. However, there are limited numbers of studies focusing on the dynamic behavior of additively manufactured lattice structure. Recently, Elmadih et al., (2017) and Syam et al., (2018) explored the dynamic behavior of lattice structure fabricated using laser powder bed fusion (LPBF) experimentally and numerically for application isolator vibration control. Next, Azmi et al., (2018) investigated the dynamic behavior of fused deposition modeling (FDM) on lattice structure experimentally for load bearing application. But, the studies on dynamic behavior of the lattice structure that fabricated AM method especially numerical approach are limited, so this study will investigate the dynamic behavior of lattice structure using numerical method and compare to the result obtained experimentally.

1.3 Objective

The objectives for this research are:

1. To obtain vibration characteristic of solid and lattice structure material bar using finite element analysis.
2. To validate the result obtain with experimental method.

1.4 Scope of Study

The scopes of study are listed as below:

1. This study includes the draw and design of the BCC lattice bar model with strut diameter size 1.0 to 1.8 mm.
2. This study analyze vibration characteristic of solid and BCC lattice bar models from ABS, titanium and stainless-steel materials using finite element method (FEM).
3. This study analyze static deflection of solid ABS and lattice ABS bar models using finite element method (FEM).
4. This study conduct modal testing of solid and BCC lattice ABS bar samples with strut diameter size 1.4 to 1.8 mm experimentally.

CHAPTER 2

LITERATURE REVIEW

2.1 Overview

In this chapter will be focusing on reviewing about the lattice structure material, vibration analysis, finite element method (FEM)

2.2 Lattice Structure Material

Lattice structure is a type of architectured material, which is a combination of monolithic material and space to generate a new structure which has the equivalent mechanical properties of a new monolithic material (Ashby, 2013).

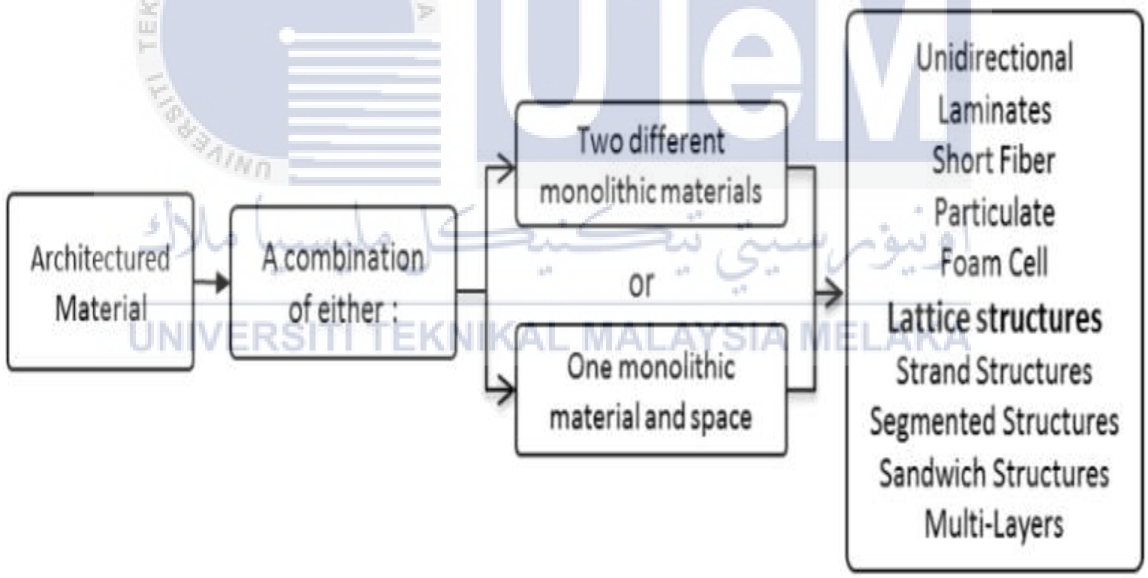

Figure 2.1:Flow of architectured materials according to (Ashby, 2013).

Figure 2.1 illustrates the combination and types of architectured materials. Other name for architectured materials is cellular structures. The word “cell” get from a latin word that call “cella”, which means enclosed space or small compartment (Gibson and Ashby, 1999).

Cellular structures come from the clusters of a cell. Wood, cork and sponges are the most common cellular structures we used in daily life. These structures have existed for ages and human beings have benefited from their various uses.

2.2.1 Lattice Structure in Nature

In nature, a lot of materials that contain lattice structure design. The materials are lightweight structures. Natural tabular structures often have honey- comb like or foam like core, that can increase the resistance of the shell to local buckling failure and supports denser outer cylindrical shell (Gibson,2005).

To form lightweight high strength materials, the configurations of lattice structure can refer from the materials. Hexagonal lattice structure is one of example that have some similarities with cellular structure of the wood. The behavior such as stiffness and strength of a species wood depends on its density and applied load. If applied load same direction with the wood, the stiffness and strength will higher be compared if the applied load across the wood. Another example is the trabecular bone. The structure of the bone is adapted to the loads applied to it. It grows in response to the magnitude and direction of the load applied (Gibson, 2005).

There are two categories divided for architectured materials which is stochastic and periodic structures. For materials that can characterize by a unit cell that can be translated through the structure are known as periodic materials (Wadley, 2002).

Cellular materials that cannot be defined by a single unit cell area are referred to as stochastic foams. Periodic cellular structures are divided into two types. First, periodic materials defined as unit cells are translated into two dimensions are known as prismatic cellular materials (Wadley, 2002). The second type are periodic materials which have 3D periodictivity. The unit's cells are translated along three axis and these structures referred to lattice materials (Wadley,2002).

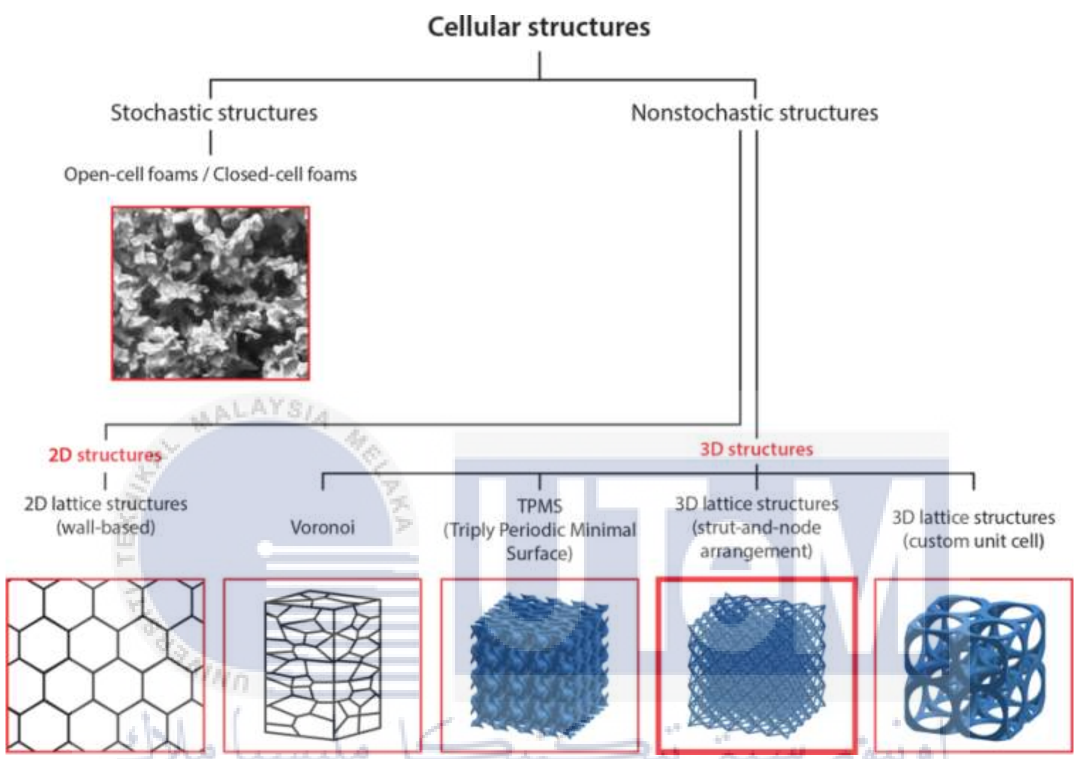

Figure 2.2: Stochastic, periodic, prismatic, and lattice structures (Azman, 2017).

2.2.2 Lattice Structure Pattern

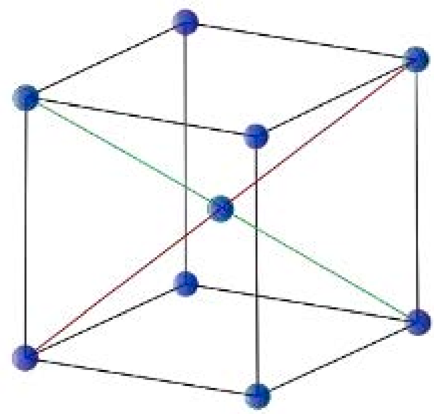

Figure 2.3: Cell of Body Centered Cubic

Figure 2.3 shows one of the types of the lattice structure pattern, there are several types. The pattern are depends on of its elementary structure. The common lattice structure topological designs are octet-truss, kagome, body centred cubic (BCC), and pyramidal etc. Octet-truss elementary structure containing an octahedral core surrounded by tetrahedral units, tetrakaidecahedron structure and open-cell foam structure (Azman, 2017).

2.2.3 Lattice Structure Properties

In material science, properties of material can be shown in different type of diagram. However, they all have one thing in common, which is that they have parts of the diagram filled with materials, and parts which have holes and are empty (Ashby, 2013). One of the example is shown figure 2.5 where the big holes in the top left and bottom right corner in the Young's modulus density space. This means that it does not exist a monolithic material which has high elastic modulus and low density.

Monolithic materials are not able to fill whole space in material science and are not sufficient to fulfill all required properties, hence creating the need of architectured material, it is possible to produce parts with high stiffness to density ratio and fill these holes of the diagram. These materials such as foams and lattice structures must be seen as a single material in its own right, with its own properties. If a cellular material outperforms an existing material in the material property diagram, then the material property space has been extended (Ashby, 2013). The possibility to fill the big holes left in this Young's modulus-density diagram with lattice structure is very interesting.

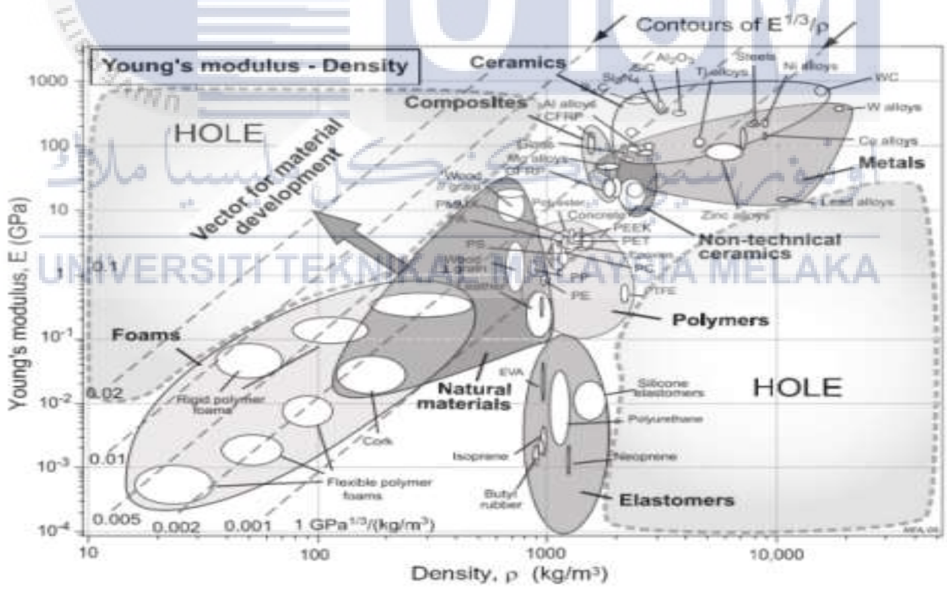

Figure 2.4: Young's Modulus-density space materials diagram (Ashby, 2013).

2.2.4 Mechanical Properties of Lattice Structure

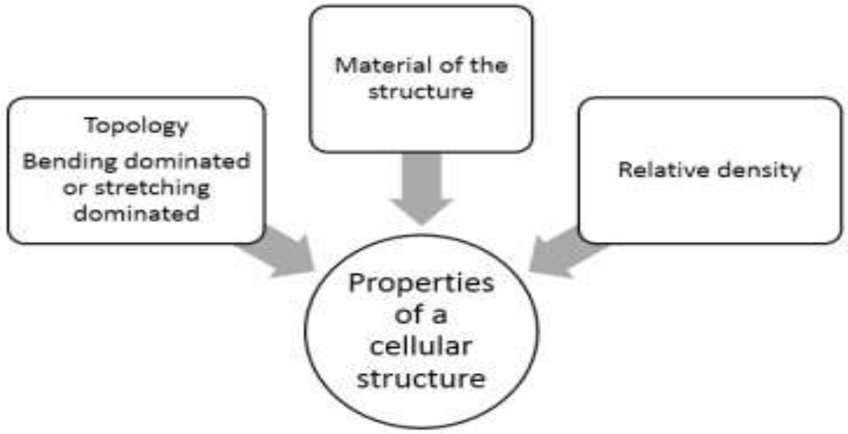

Figure 2. 5: Three main lattice structure design variable influence according.

The properties of the structure are influence by the three main factors which is the material of the structure, its cell topology and its relative density (Ashby, 2006). This is shown in figure 2.6. For mechanical, thermal and electrical properties are depending on the material that made for lattice structure. Whereas the elementary structure pattern or topology influences the bending-dominated or stretching-dominated property of the structure. The strut size and length are influenced the relative density. The relative Young's modulus of a bending-dominated structure scales with square of the relative density.

Prismatic structures have single properties which are only in one direction of the part. Whereas lattice structures can have multifunctional properties and along each X, Y and Z axis of the part. Another interesting possibility is to create a lattice structure which has different mechanical properties for each direction of the part, depending on the requirements of the part in each direction.

To help differentiate the lattice structure mechanical properties and its applications, these structures can be categorized in two different deformation categories: bending dominated and stretching-dominated structures. Stretching-dominated is useful to produce high stiffness and low weight parts, for example cubic and octet-truss lattice structures. On the other hand, by orienting the lattice structures struts in a certain pattern to obtain a bending dominated structure, it is also possible to manufacture parts suitable for energy absorption (Evans et al., 2001). The design pattern of a lattice structure influences its mechanical property. This information (Suard, 2015) is summarized in table 2.1 for each lattice structure pattern.

Table 2.1: Type of deformation for lattice structure according to (Suard, 2015).

Features	Cubic	Octet-truss	Tetrakaidecahedron	Open-cell foam
Type of deformation	Stretching dominated	Stretching dominated	Bending dominated	Bending dominated
Application	For high stiffness low mass part	For high stiffness low mass part	For high energy absorption parts	For high energy absorption parts

The difference between stochastic and periodic structure mechanical properties influences their applications. Stochastic foams are bending-dominated structures, thus are well equipped for energy absorption.

2.2.5 Manufacturing Method of Lattice Structure

In this section will review about the manufacturing process of lattice structure. For method there have two types which is conventional method and modern method.

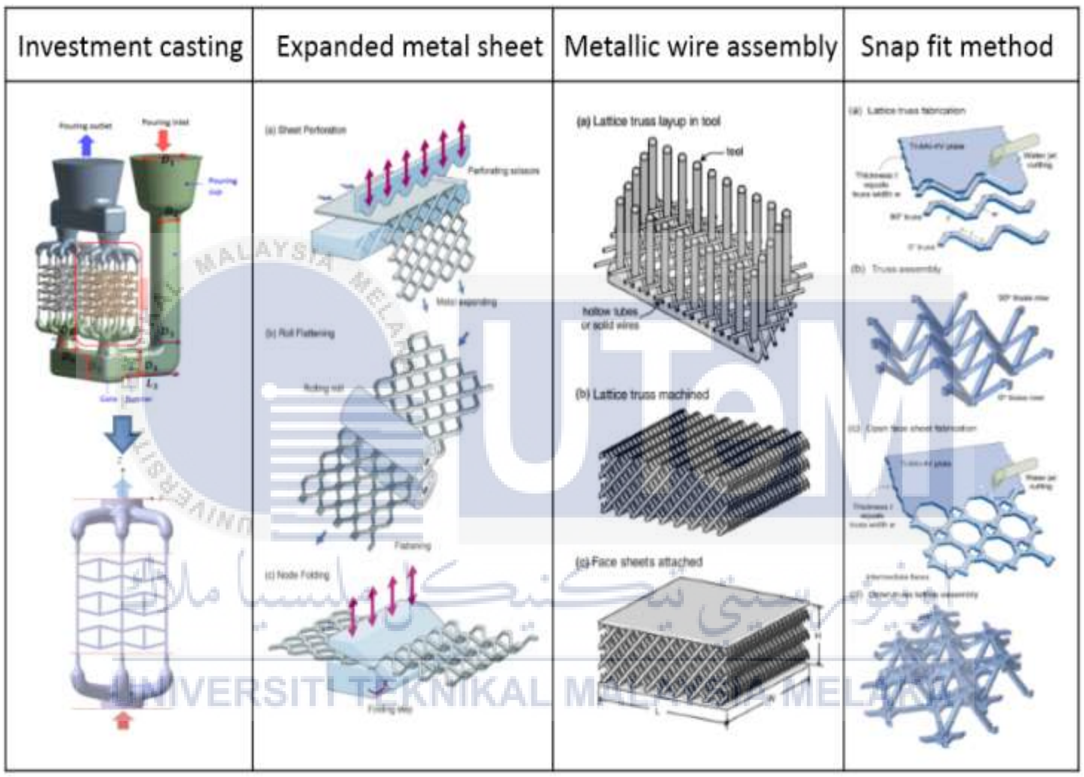

Figure 2.6: Conventional method of Lattice Structure (Azman, 2017).

For conventional method there have four method which is investment casting, expended metal sheet, metallic wire assembly and snap fit method as shown in figure 2.7. Table 2.2 illustrates the basic step for each method of manufacturing lattice structure.

Table 2.2: Step of process of each conventional Method.

Method	Step
Investment Casting	1. Assembled the pattern and dipped into the ceramic slurry to obtain a ceramic shell coating. 2. Dry and dewax of the pattern assembly. 3. Crack the pattern to obtain the final product.
Expended Metal Sheet	1. Cutting 2.flattening 3. Folding
Metallic Wire Assembly	1. Stainless steel solid wires and hollow tubes are gathered using tooling to align the cylinders in collinear layers. 2. Orientation alternates for each layer to form the lattice's structure. 3. Brazzing to obtain the structure.
Snap Fit Method	1. Metal sheets were cut with water jet according to the truss shape. 2. Rows of the trusses were aligned and snap-fit attached to the structure to form the octet-truss lattice structure. 3. Brazed the lattice structure for bonding

For modern method additive manufacturing (AM) is the method that used to produce lattice structure pattern. The many type of AM technologies. These can be categorized into two categories, either layer-based or direct deposition (Vayre et al., 2012). Examples of layer-based additive manufacturing are selective laser sintering (SLS), selective laser melting (SLM) and electron beam melting (EBM). The two types of energy sources used to melt the metallic powders for additive manufacturing machines are laser and electron beam. The techniques which fully melt the particles are SLM and EBM. Whereas the processes which partially melt the particles are SLS and direct metal laser sintering (DMLS) which can make strong part. Only EBM and SLM are capable of manufacturing metallic lattice structures. Other AM techniques are stereolithography (SLA), laminated object manufacturing (LOM) and fused deposition modeling (FDM) which can fabricate reliable plastic parts. From the all AM techniques that stated before, the FDM technique is the simplest. Thus, this will make the fabrication cost significantly lower while still making reliable and strong plastic parts (Azmi et al., 2017).

2.2.6 Research on Lattice Structure

There are many research articles on lattice structure. In early decades, the physical properties of lattice structure have been studied. In the early stage, (Gibson et al., 1982) investigated the mechanical properties of two-dimensional (2D) and 3D cellular materials with beam theory. It was found that the effective Young's modulus was controlled by the relative density of the cellular material.

The increasing of experiment on lattice structure after the additive manufacturing (AM) is to be used to fabricate lattice structure. More complicated experiment on lattice structure have been done. Labeas and Sunaric (2010) conducted compressive experiments to understand the static response and failure process of lattice structures made of Stainless Steel 316L. The result showed that the structural response was strongly influenced by the strut geometrical characteristics such as the aspect ratio, the unit-cell size, and the shape.

Next, Alsalla et al. (2016) investigated the fracture toughness of Stainless steel 316L lattice structures through tensile tests. It was found that the result was highly influenced by the building orientation. The horizontal struts were weaker than the struts built in the vertical direction.

Meanwhile, Yang et al. (2012) investigated the flexural property of auxetic lattice structures through bending tests by design the sample using electron beam melting (EBM) and selective laser sintering (SLS). The result indicated that the flexural strength of auxetic lattice structures was higher than regular sandwich panel structures.

Furthermore, impact loading tests (Winter et al., 2014), dynamic tests (Salehian and Inman, 2008), and fatigue test (Jamshidinia et al.,2015) have also been conducted to investigate the performance of lattice structures fabricated by different types of AM techniques.

2.3 Introduction Vibration

Vibration is physical movement or motion of rotating machine is normally referred to as vibration. By using sight or touch sense the vibration frequency and amplitude are cannot be measured. That's means must be employed to convert the vibration into a usable equipment that can be measured and analyzed. The different form of vibration can be sensed by seeing and touching (Vishnu, 2015).

The term vibration also can relate in mechanical engineering. Therefore, the vibration in mechanical engineering is often associated with a system that can swing freely without the applied force. Next, vibration also can cause the minor problem to serious and threatened security in engineering system. For example, in plane when the plane flying in the air, the plane's wings will vibrate. This will cause the passengers will not comfortable with that situation, especially when the frequency of vibration in accordance with the original frequency in the human body and organs. In fact, if this had not prevented vibration it can cause serious internal injury due to the passenger. Besides that, the current cost of designing aircraft are to exposure to vibration (Clevenson et al., 1978).

Vibration also related to the dynamic analysis, there is two type of analysis which is static and dynamic analysis. Structural analysis is primarily related to finding out when introduced to load the behavior of a physical structure. The loads can originate from the weight of the physical structure itself, people standing on it, large heavy furniture etc. or from external or ambient loads such as earthquake, wind or ground shaking from machines operating nearby the structures. The difference between the static and dynamic loading in analysis on the physical structures is that in the static analysis the load is applied 'slowly' where the time and inertial effect are not relevant to the analysis and thus simplified whereas in the dynamic analysis the load is applied over time or at certain frequency making time and inertial effects are relevant to the analysis. In other words, in the static analysis, the frequencies of the loads applied to the physical structure are much smaller than the natural frequencies of the structure, while in the dynamic analysis the load applied has sufficient acceleration where the frequency range is in the range of comparison relative to the natural frequencies of the structure. Dynamic analysis is also related to the loads experienced by a physical structure when it is excited by suddenly applied dynamic loads as some loads are not present at some point in time. Therefore, structural dynamic analysis is a type of structural analysis that covers the behavior of structures subjected to dynamic (high acceleration) loadings. Structural dynamics testing and analysis contributes to progress in many industries, including aerospace, automotive, manufacturing, wood and paper production, power generation, defense, consumer electronics, telecommunications and transportation (Mahmood et al., 2017). Dynamic analysis can be used to detect dynamic displacements, time history and modal analysis. Forced vibrations occur when the object is driven by external force to vibrate Vibration continues forever, as long as the driven force still exists. Consider a single degree of freedom (SDOF) mass spring damper (MSD) consisting of mass, spring and damper element as shown in Figure 2.17 for lumped parameter system.

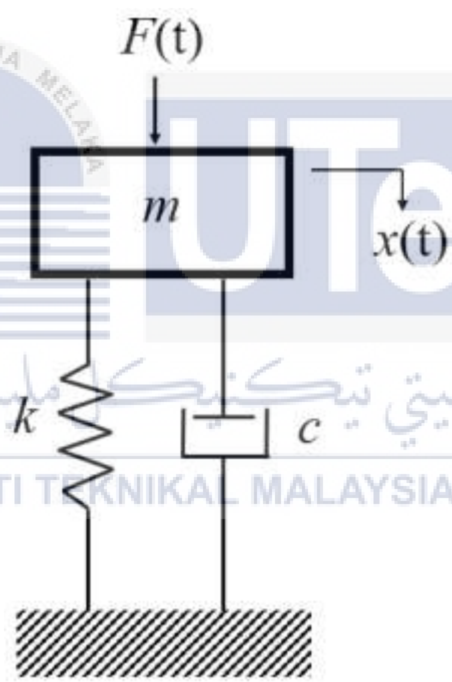

Figure 2.7: An illustration of MSD model of a SDOF system.

For harmonic force, the equation of motion as complex equation is as follow:

$$m\ddot{x}(t) + c\dot{x}(t) + kx(t) = Fe^{jwt} \tag{2.1}$$

where m is the mass, k is the stiffness, c is the damping factor, $\ddot{x}$ is the acceleration, $\dot{x}$ is the velocity, x is the displacement and F is the force. Here, the real part of the complex solution corresponds to the physical solution $x(t)$. By assuming the complex solution of equation (2.1) is of exponential form

$$x_p(t) = Xe^{jwt} \tag{2.2}$$

by substituting equation (2.2) into (2.1), equation (2.1) becomes

$$(-\omega^2 m + cj\omega + k)Xe^{jwt} = Fe^{jwt} \tag{2.3}$$

by cancelling the e^{jwt} yields

$$X = \frac{F}{(k-\omega^2 m+c\omega j)} \tag{2.4}$$

by rearranging gets

$$\frac{X}{F} = \frac{1}{(k-\omega^2 m)+(c\omega j)} \tag{2.5}$$

the equation (2.5) is known as the (complex) frequency response function (FRF). By multiplying equation (2.5) to its complex conjugate yields the magnitude of the FRF

$$\left|\frac{X}{F}\right| = \frac{1}{\sqrt{(k-\omega^2 m)^2+(c\omega)^2}} \tag{2.6}$$

and the phase of the FRF

$$\emptyset = tan^{-1}\left(\frac{c\omega}{k-\omega^2 m}\right) \tag{2.7}$$

Figure 2.18 shows the SDOF system's FRF and bode-plot graphs. FRF are typically transfer functions used in vibration analysis and modal testing. The FRF expresses the structural response ratio as output to force applied as input. Figure 2.18 shows that the magnitude is amplified and the bode plot has a sharp phase shift at an angle of 90 ° when the frequency of the output force (operating frequency) is equal to the natural frequency of the system. The peaks in the FRF graph and the sharp phase shift at 90 ° angle in the bode-plot graph specified the system's natural frequency. There are several basic transfer functions based on the response measurement as outlined in Table 2.3.

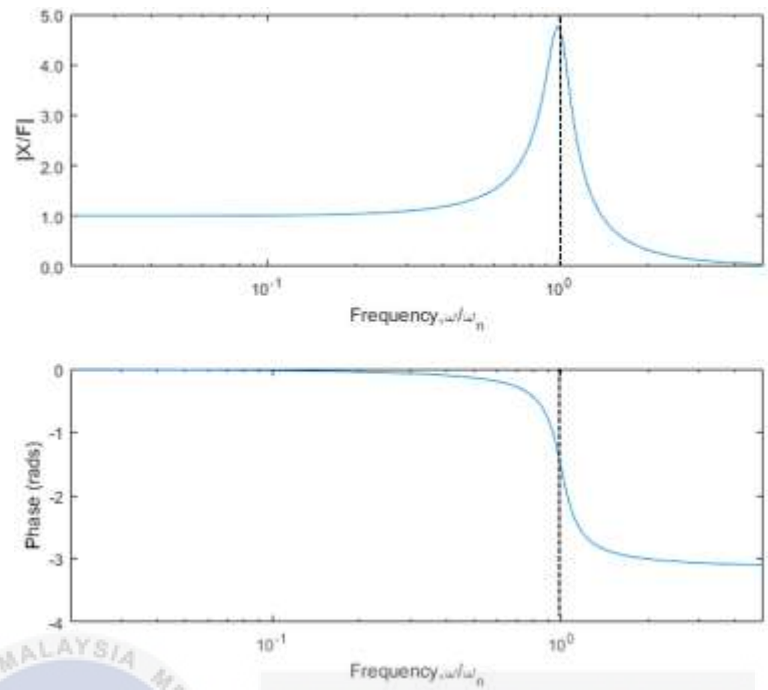

Figure 2.8: FRF and bode-plot graphs of a SDOF system with m=2000 kg, k= 45 kN and C= 2000 s□N/m

Table 2. 3: Transfer functions used in vibration measurement (Irvine, 2000; Inman and Singh, 2014)

Response measurement	**Transfer function**	**Inverse transfer function**
Displacement	Receptance	Dynamic stiffness
Velocity	Mobility	Impedance
Acceleration	Accelerance	Apparent mass

2.4 Vibration Analysis

Vibration Analysis applied in an industrial or maintenance environment aims to reduce maintenance costs and equipment downtime by detecting equipment faults. Vibration analysis is a main component of a condition monitoring (CM) process and is often referred to as predictive maintenance (PdM). Application of vibration analysis are most commonly is used to detect faults in rotating equipment (Fans, Motors, Pumps, and Gearboxes) such as Unbalance, Misalignment, rolling element bearing faults and resonance conditions. Vibration analysis can use the units of displacement, velocity and acceleration displayed as a time waveform (TWF), but most commonly the spectrum is used, derived from a Fast Fourier Transform of the TWF. The vibration spectrum provides important frequency information that can pinpoint the faulty component.

Vibration analysis is a process of looking for anomalies and monitoring change from the established vibration signature of a system. The vibration of any object in motion is characterized by variations of amplitude, intensity, and frequency. These can correlate to physical phenomena, making it possible to use vibration data to gain insights into the health of system or equipment. Vibration analysis is a very wide and complex domain which exploits several aspects of the testing and diagnosis disciplines, from condition monitoring to defect detection (Larizza, 2015). Due to the improvement of sensor technology now permit the use of vibration analysis methodology within the very small size (micro) component. Noncontact high-speed (wide bandwidth) laser sensors (typically displacement sensors) can overcome the traditional limits exhibited by accelerometers, so highly accurate and localized analyses can be performed (Larizza, 2015). From the table 2.3 shows the four principal domains of vibration analysis methodology.

Table 2.4: The principal domains of vibration analysis.

Principal Domains	Function
Time domain	-Detecting the integral performance of the tested part: peak, average, root-mean-square, envelope values of vibration amplitude. These values are compared with threshold values in order to detect abnormal performance or latent defects.
Frequency domain	- provide more information as the measured signal is decomposed into a sequence of frequency components (spectrum)
Joint domain (time/frequency domain)	- In a particular case of time/frequency analysis, the spectrums are related to the rotational speed of the tested devices (order analysis), such that the analysis of the single order which is represented by a frequency component varying with the speed is rendered possible.
Modal analysis	- the study of the dynamic properties of structures under vibration excitation. This technique uses FFT in order to carry out a transfer function which shows one or more resonances, by means of which it is possible to estimate the characteristic mass, damping, stiffness, and other properties of the tested part.

2.4.1 Research Vibration Analysis on Plate

For vibration analysis on plates there are many research articles. Burlayenko et al. (2015) study to find out the weaknesses and strengths of each model used and to pick out their interchangeability for the finite element calculations by different plate finite element models used for the free vibration analysis of homogeneous isotropic and anisotropic, composite laminated and sandwich thin and thick plates with different boundary conditions. The result shows the finite element model depends on the accuracy and available numerical possibilities. Besides that, finite element technique is a method based on an idealization of geometry and mesh sensitivity need to be considered.

Aerospace vehicle such as aircraft, rockets, and missiles most commonly used stiffened laminated plate. Rajawat et al. (2017) were done free vibration analysis of stiffened laminated plate using finite element method and the simulation using ANSYS. The aim of the research to determine structural deformation and vibrational characteristics of stiffened laminated plate where must have high natural frequencies. The result that obtain in that research compared with the results stiffened composite plate. The result shows that the present model of stiffened laminated plate gives quite accurate result to the stiffened composite plate.

Next, Liew et al. (2009) have explored a mesh-free Galerkin method for free vibration analysis of unstiffened and stiffened corrugated plates. From the analysis carried on the stiffened corrugated plates, treated as composite structures of equivalent orthotropic plates and beams, and the strain energies of the plates and beams are added up by the imposition of displacement compatible conditions between the plate and the beams. The stiffness matrix of the whole structure was derived.

2.4.2 Research Vibration Analysis on Beam

Since vibration analysis also important to the beam structure they many research have done on beam structures. In the early stage, Maurizi and Belles (1993) determined natural frequencies of metallic beams with one step change in cross section.

Jen and Magrab (1993) obtained an exact solution for the natural frequencies and mode shapes for a beam elastically constrained at its end and to which a rigid mass is elastically mounted. The results show, the differences between the results obtained using approximate methods and the exact solution can sometimes be very large. The manner in which the numerical results were presented clearly show the effects that the two degree of freedom system's parameters and location have on the beam's lowest natural frequencies and the conditions under which the attached system essentially uncouples from the beam.

Dong et al. (2005) presented a scheme to calculate the laminated composite beam flexural rigidity and transverse shearing rigidity based on first order shear deformation theory. A stepped beam model was then developed using Timoshenko’s beam theory to analytically predict the natural frequencies and mode shapes of a stepped laminated composite beam

Vaz and Junior (2014) study the natural frequencies and the mode shapes of beams with variable geometry or material discontinuities. By using Euler-Bernoulli beam theory in order to evaluate the natural frequencies and the mode shapes of stepped beams in multiple parts. The result obtains the comparison between calculated and measured frequencies and their show good agreements, since the percentage of difference are small.

2.4.3 Research Vibration Analysis on Lattice Structure

Since this study will focused on lattice structure material, some research that have been done before in vibration analysis, but still not enough works investigate on the dynamic behavior of lattice structure material. Li et al. (2006) study the effects of local damage on the vibration characteristics of different composite lattice truss core sandwich structures by using uniform load surface (ULS) curvature, and developed according to the synergy of gapped smoothing method (GSM) and Teager energy operator (TEO), which is denoted as GSM-TEO method. The result on experiment and numerical solution demonstrated that the GSM-TEO methods are reliable and applicable for damage localization in composite lattice truss core sandwich structures.

Lou et al. (2014) was investigated the effects of local damage, in the form of missing part of the truss members, on the natural frequencies and the corresponding vibration modes of composite pyramidal truss core sandwich structures experimentally and numerically. From the investigation shows that the structural natural frequencies decrease due to the loss of stiffness caused by the existence of local damage of the truss core. Next, the vibration modes of the damaged composite pyramidal truss core sandwich structures show obvious local deformation in the damaged region and the effects of local damage on structural natural frequencies get smaller as the damaged region.

Elmadih et al. (2017) are focused on applications of lattice structures for vibration isolation by using various configurations of strut-based lattice structure. The result shows the natural frequency of a lattice structure can be reduced by increasing cell size, reducing volume fraction.

2.5 Finite Element Analysis

The Finite Element Analysis (FEA) is the simulation of any given physical phenomenon using the numerical technique called Finite Element Method (FEM). Engineers use it to reduce the number of physical prototypes and experiments and optimize components in their design phase to develop better products, faster. Finite element analysis (FEA) is a numerical method used to solve engineering field problems by dividing a domain into several smaller finite subdomains, which each act as individual elements over which algebraic equations are applied and an approximate solution is given using the finite difference method

(Russel, 2013). The results from each finite element are then reassembled and different types of analysis can be run to solve any number of complicated engineering problems using this method and a powerful solver (Reddy, 2006). The mathematical theory and application of the method are vast (Budynas and Nisbett, 2011). There is also a number of commercial FEA software packages that are available, such as ANSYS, NASTRAN, ABAQUS, and LS-DYNA.

2.5.1 Application of Finite Element Analysis

There are a many function of FEA applications such as static and dynamic, linear and nonlinear, stress and deflection analysis, free and forced vibrations, heat transfer (which can be combined with stress and deflection analysis to provide thermally induced stresses and deflections). Figure 2.7 shows the example application of finite element analysis. The basic method by which a problem is solved using FEA can be broken down into several steps (Cook, 2007). First, the problem must be identified and classified. There are several different types of analysis that can be performed. Selecting the correct analysis for the correct problem is important. Next, a simplified mathematical model should be derived from which to build the basic physical concepts of the analysis. Preliminary analysis is then performed, in which a solution is obtained to help ballpark the result sought after from the FEA study. The next step is to actually perform the finite element analysis, which is almost always done with the aid of a computer. The final step is to check the results. It is significant to first note if the results "look" correct, if they make sense, and if they are similar to the preliminary analysis performed. It may also be necessary to check the results against other solution forms, or against a physical model (Cook, 2007). It must also be noted that the FEA process is a very iterative one. Rarely is the first FEA study the final one and revisions are often needed after interpreting the results of a study.

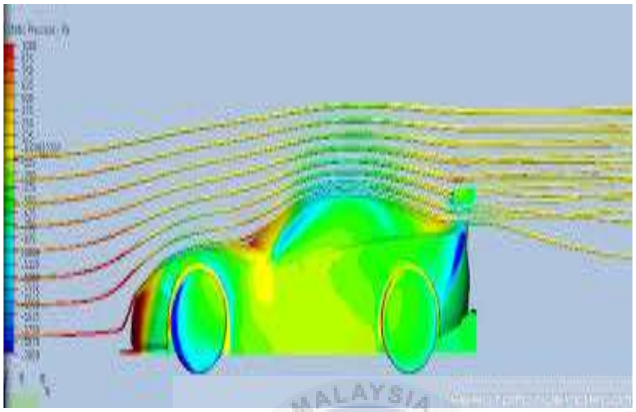

(a)

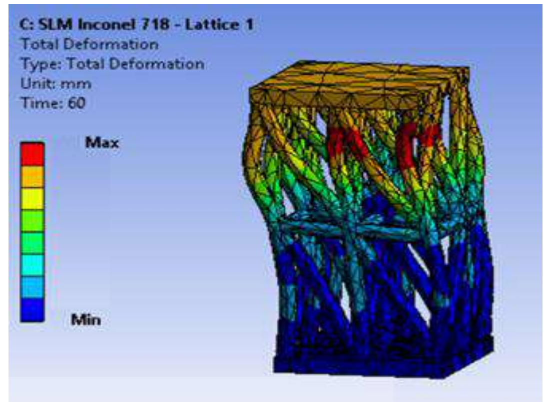

(b)

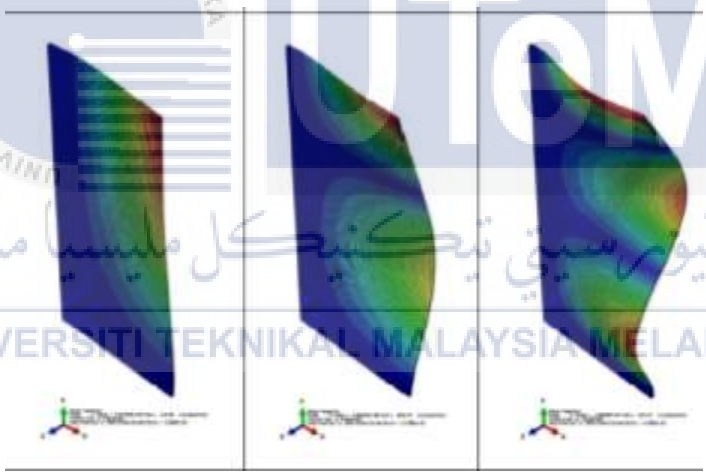

Figure 2.9: (a) CFD on streamline of car; (b) Static analysis of stress distribution (Vannutelli, 2017) and (c) Dynamic analysis of vibration mode shape (Ismail, 2013).

2.5.2 Finite Element Analysis Using ABAQUS/CAE 6.14.1

In this study, finite element analysis using ABAQUS/CAE 6.14.1 is undertaken to investigate the vibration of lattice structure. ABAQUS can solve problems of relatively simple structural analysis to the most complex linear and nonlinear analyses. In ABAQUS, there are some intrinsic methods that can be used to achieve dynamic analysis (Ismail, 2013). There are two basic types of direct integration methods existing in ABAQUS, namely, i) Implicit Direct Integration which is provided in ABAQUS/Standard and ii) Explicit Direct Integration provided in ABAQUS/Explicit.

2.5.3 Finite Element Analysis On Lattice Structure

There are many researches in lattice structure case using FE analysis in order to compare the numerical result with experimental result. Wallach and Gibson, (2000) have modeled a sheet of lattice structures with a thickness of one unit-cell, which is the building block for the lattice structure. The work was concerned with analytically modeling the elastic properties of the sheet and assumed that the struts of the lattice structure are connected with pin joints, which allows only axial loading on the struts of the lattice structure. The sheet was subjected to axial loading in the x, y and z directions and the results were compared with experimental results giving an error percentage of 3% to 27% depending on the loading direction.

Johnston et al., (2006) analyzed the octet-truss unit-cell with the hypothesis that the struts perform like beams, which allowed the inclusion of bending, shearing and torsion effects on the structure. The unit-cell was investigated using a unit-truss model that consists of a central node with set of half-struts linked to it and a common strut between two next unit-trusses. The results had a relative error of less than 10%.

Li et al., (2015) was studied of the debonding of truss bar in composite lattice truss core sandwich structures by using gapped smoothing method - teager energy operator (GSM-TEO) method and uniform load surface (ULS). The effects of local damage on the vibration behavior of different composite lattice truss core sandwich structures are firstly studied, and then, experiment and numerical simulation are conducted to measure the performance of the suggested method. The results show a relative error is less than 13%. Figure 2.8 shows the vibration mode shape using finite element analysis in the study.

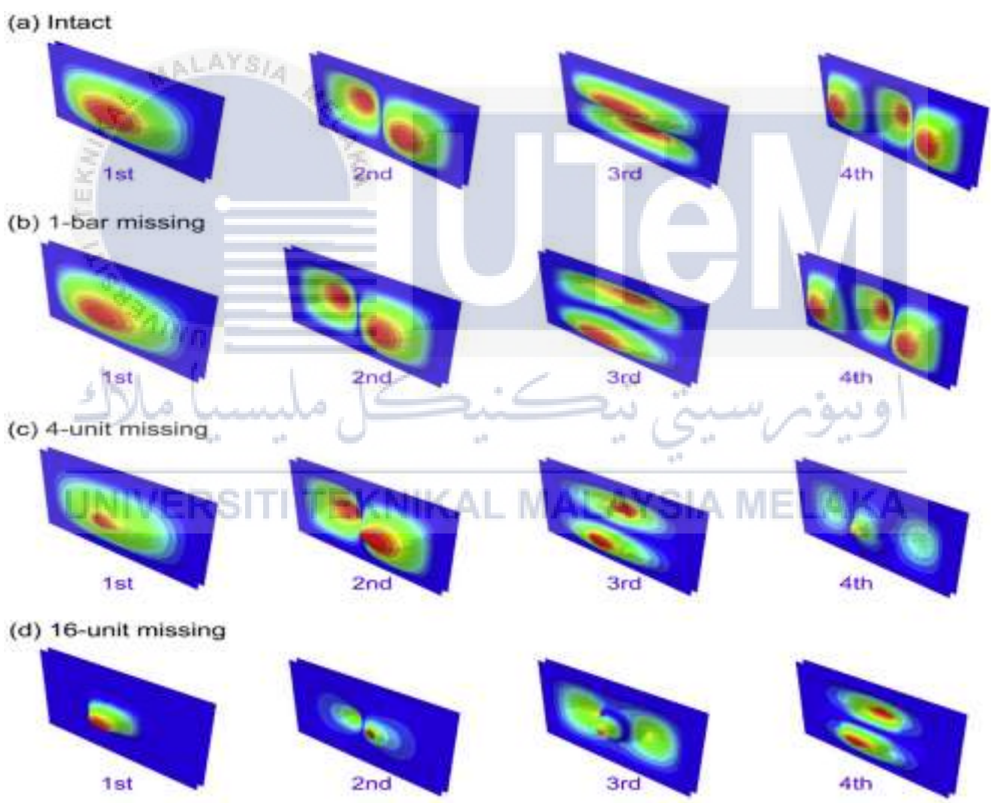

Figure 2. 10: First four order mode shapes of composite tetrahedral truss core plate (Li et al., 2015).

Elmadih et al., (2017) was studied the dynamic behavior of many configurations of strut-based lattice structure fabricated using additive manufactured. As resulted in the experiment and numerically show the relative error is less than 10.2%. Lattice structures can be used to tune the design of a structure to have a desired natural frequency for a specific vibration isolation application, effectively setting up a mechanical band-gap.

CHAPTER 3

METHODOLOGY

3.1 Overview

This chapter presents the sequence of this study. For ease, the flow of the methodology of this study is summarized in Figure 3.1. The calculation to get the design parameter also presented in this chapter. Besides that, the designing steps of the lattice structure by using SolidWorks software is also described here. In addition, steps to perform the vibration modal analysis and static analysis using the ABAQUS finite element analysis (FEA) software.

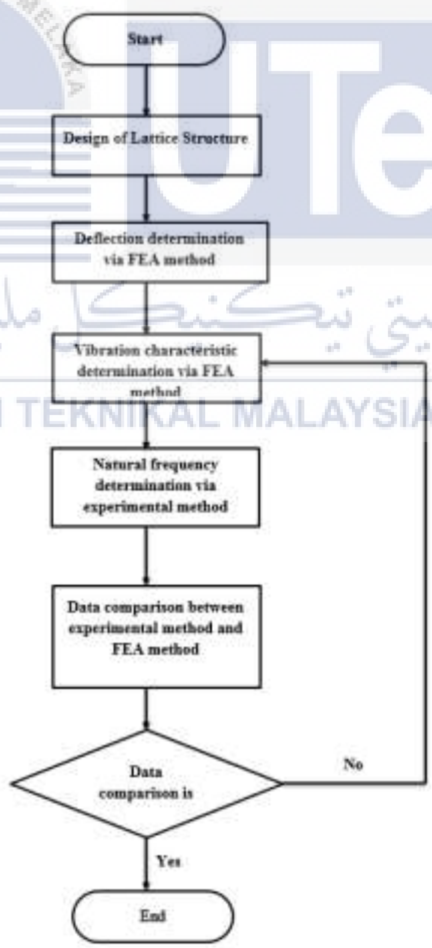

Figure 3.1: Flow chart of general methodology.

3.2 General Methodology

The phases involved for the completion of this research are as follow:

1. Project planning and literature review
    - Planning the timeline of the research and to gather resources and information from related articles, journals or any materials.
2. Design of lattice structure
    - Design of the lattice structure using SolidWorks.
3. Static deflection analysis using FEA
    - Obtain the deflection of ABS solid model and ABS lattice model.
4. Vibration characteristics characterization using FEA
    - Obtain the vibration characteristic using ABAQUS finite element analysis (FEA) software.
5. Natural frequency determination using modal analysis
    - Conduct an experiment of vibration testing to get the natural frequency of ABS solid and ABS lattice samples.
6. Data analysis
    - Analyze the data obtained from the ABAQUS finite element analysis (FEA) software.
7. Data Comparison with experimental results
    - Compare the data analysis from ABAQUS finite element analysis (FEA) software with the experimental results.

3.3 Design of Lattice Structure

3.3.1 Design Parameter of Lattice Structure

Prior to the drawing stage using SolidWorks software, there are some important parameters that must be defined. The parameters calculation are shown afterwards.

<u>Calculation (Based on Figure 3.2 and 3.3)</u>

Diameter chosen = 1.4mm ,1.6mm, 1.8mm

Dimension of lattice structure cube block = 20 mm x 20 mm x 20 mm

Number of unit cells in a cube block = 4 layers

Edge length of one unit cell, X = 20 mm / 4

= 5 mm

Length of half unit cell, X/2 = 5 mm / 2

= 2.5 mm

Figure 3.2: Calculation of hypotenuse base length (Y) BCC structure.

Hypotenuse base length, Y $= (X^2 + X^2)^{1/2}$

$= (5^2 + 5^2)^{1/2}$

$= 7.07107$ mm

Base length of half unit cell, Y/2 $= (7.07107 \text{ mm}) / 2$

$= 3.5355$ mm

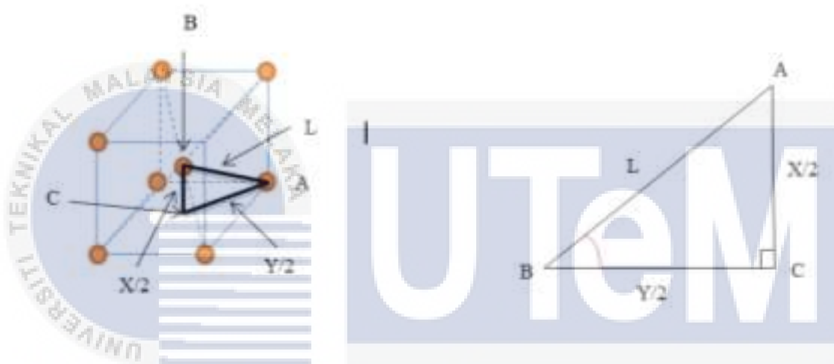

Figure 3. 3: Calculation of BCC structure for strut length (L).

Length of strut, L $= [(X/2)^2 + (Y/2)^2]^{1/2}$

$= [(2.5)^2 + (3.5355)^2]^{1/2}$

$= 4.3301$ mm

Angle ∠ABC $= \tan^{-1} (X/2) + (Y/2)$

$= \tan^{-1} (2.5) + (3.5355)$

$= 35.36°$

3.3.2 Design of Lattice Structure

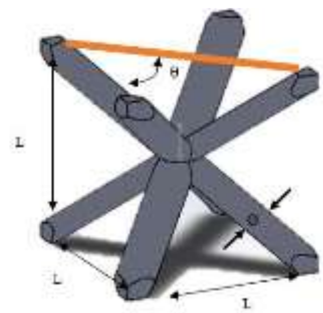

Figure 3. 4: BCC unit cell (Azmi et al., 2018).

Figure 3.4 shows the BCC one unit cell of lattice structure design which is the length, L and the surface angle are 5mm, 35.26° respectively. For the strut diameter, Ø there use five different sizes which are 1.0, 1.2, 1.4, 1.6 and 1.8mm. The size of the design lattice structure bar is 160 x 30 x 15 mm as show in Figure 3.5.

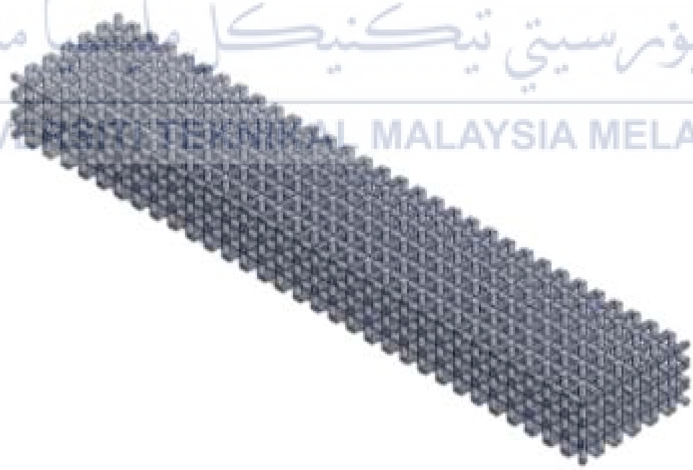

Figure 3.5: Lattice structure bar (Azmi et al., 2018).

3.3.3 Design Step of BCC Lattice Structure

1. Sketching the strut of lattice structure design

- Initially, the first step needs to open the SolidWorks software and create new document then choose the part to create the 3D single component. Next, click sketch then select the front plane to start the sketching. Draw a triangle with the dimension as shown in Figure 3.6. Afterward, as shown in Figure 3.7 before exit from the sketch mirror is needed to complete sketching on the front plane. To complete the sketching, select the right plane as a sketch plane and repeat the step like sketch on the front plane. Figure 3.8 shows the complete sketching.

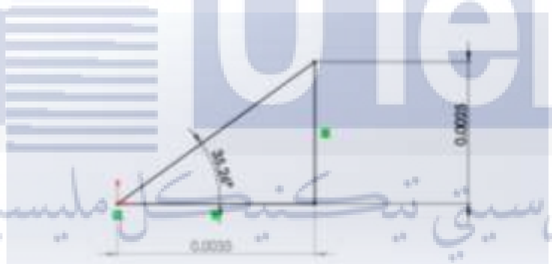

Figure 3.6: Line sketching with dimension.

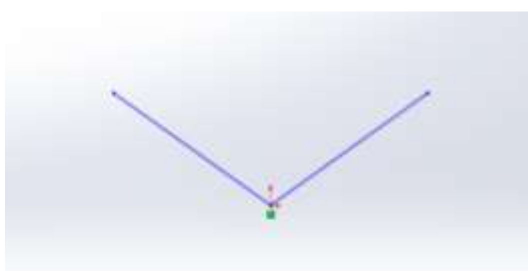

Figure 3.7: Mirror line.

Figure 3.8: Line sketching in front and right plane.

2. Extruding the strut

- In this step, the reference plane needs in order to draw a circle tangent to the line by selecting the line as a first reference and the vertex of line as second reference as shown in Figure 3.9. After creating the reference plane, draw a circle tangent to the line and extrude the circle with two directions as shown in Figure 3.10. Repeat the step for each line to complete extruding of strut. As shown in Figure 3.11 the complete extruding strut after rotate with 45 degree.

Figure 3.9: Reference plane perpendicular to sketching line.

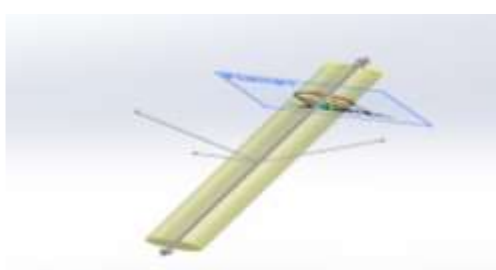

Figure 3.10: Extruding strut in two directions.

Figure 3.11: Complete strut after extrude.

3. Extruded cut the strut

- To get one-unit cell of BCC lattice structure design, the extruded cut features need to apply in this design. Firstly, need to make a reference plane. By choose front plane as first reference and offset the reference plane 2.5mm this step illustrated in Figure 3.12. Next, draw a square on new reference plane and apply cut extrude. After that, mirror the cut extrude features and select the top plane as mirror plane as shown in figure 3.13. Repeat the step for the right and front plane to complete the design one unit cell of BCC lattice structure that shows in Figure 3.14

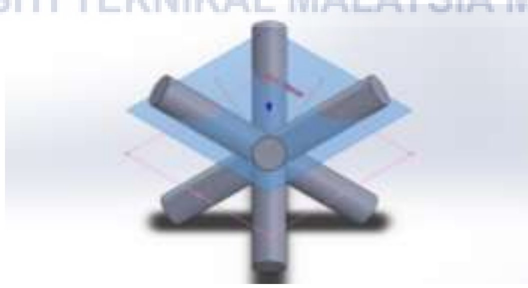

Figure 3.12: Reference plane on the top plane.

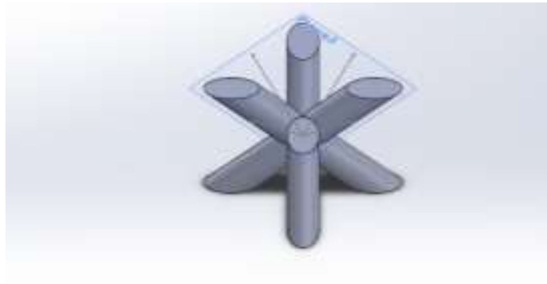

Figure 3.13: Cut extrude feature on the reference plane.

Figure 3.14: Final BCC unit cell design.

4. Mirror and combine the unit cell of BCC lattice structure

- In the final stage in design of lattice structure bar design with dimension 160mm x 15mm x 30mm. Mirror feature are used to complete the design. To create repeated unit cell, select the linear pattern and choose mirror the unit cell and combine all. In this step first step mirror along the y-axis until get 6 repeated unit cell equivalent to 30mm width as shown in Figure 3.15 and combine all become one body. Next, mirror along the x-axis until get 32 row equivalent to 160mm long and combine it. Figure 3.16 show a layer of lattice structure bar design. Finally, add another two layers by using mirror feature and combine all layers to complete the design of lattice structure bar as illustrated in Figure 3.17. Save the design and convert to step file or parasolid format in order to export onto ABAQUS software.

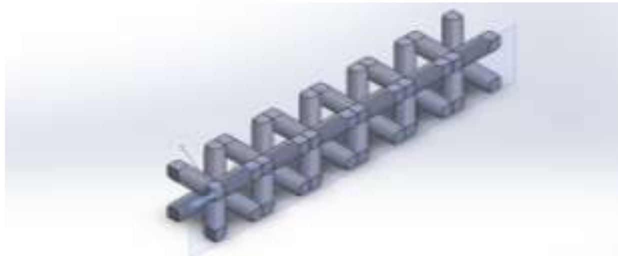

Figure 3.15: Width of lattice structure.

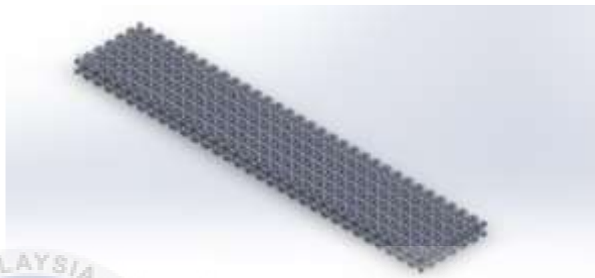

Figure 3.16: First layer of the lattice structure.

Figure 3.17: Lattice structure bar design.

3.2 Numerical Solution of Lattice Structure

In this section show the step that required performing the finite element analysis by using ABAQUS/CAE 6.14.1 software. The lattice structure model is 160 x 30 x 15 mm. The material and element properties are show in Table 3.1.

3.2.1 Step of FEA Using ABAQUS/CAE 6.14.1

1. Design of part

- Firstly, the lattice structure bar is designed in three-dimensions (3D) by using SolidWorks 2016. The step file is imported into the ABAQUS working environment and part attributes section choose deformable types.

2.Build the material description

- This step defines the material in the Property module. First, create material then select general and picked density. Next, select mechanical and picked elasticity. The value of the properties such as density, poison ratio and modulus of elasticity are listed in Table 3.1.

Table 3.1: Property of lattice structure.

Property name	**Details**		
Material	ABS	Titanium	Stainless steel
Density	1050 kg/m^3	4430 kg/m^3	8000 kg/m^3
Young's Modulus	3 x 10^9 N/m^2	114 x 10^9 N/m^2	193 x 10^9 N/m^2
Poison Ratio	0.35	0.33	0.28
Element Name	C3D10H – Quadratic solid element		
Geometric Order	Quadratic		

3. Definition and assignation of the section properties

- For this step need to create solid homogenous section and perform section assignment of the part in the same module which is property module.

4. Assembly the model

- In the Assembly module one creates a new part instance by click the create instance. Select part and set dependent on instance type.

5. Arrangement of the analysis

- For this section show the step for the analysis using the step module.
  i. Firstly, in step manager section click create then set linear perturbation type and select frequency. To determine the vibration modes of the lattice structure need to use frequency extraction analysis. The standard Lanczos method (ABAQUS, 2011) has been applied to extract the natural frequencies and mode shapes for the lattice structure. The frequency range allows for 10 vibration modes to be identified.
  ii. In order to obtain the deflection of the FE models. The static analysis is used. Initially, in the step manager click create then set general and select static, general.

6. Setting on boundary condition and force.

- For frequency extraction analysis the boundary condition in this analysis is set to clamp-free (CF). The clamped surface applies 20 mm parallel to *x*-axis on the upper and bottom surface of lattice structure as illustrated in Figure 3.18.

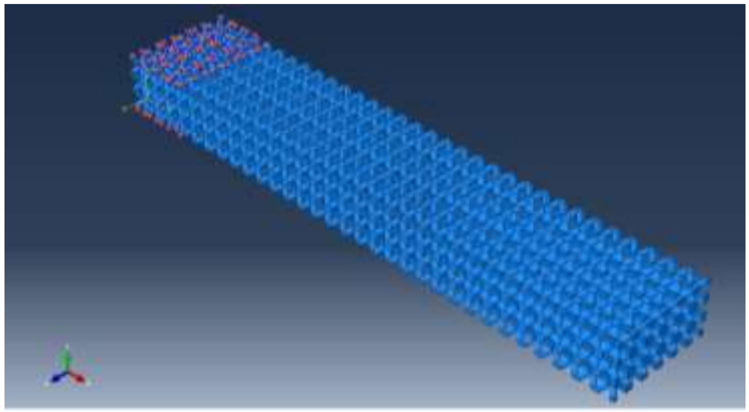

Figure 3.18: CCFF boundary condition

- For deflection extraction analysis, a concentrated force of 1 N to 10 N with increment 0.5 N is applied to lattice structure and Solid ABS at distance 145 mm in the x-direction and 15 mm in the y-direction as shown in Figure 3.19 to use in deflection extraction analysis for ABS material.

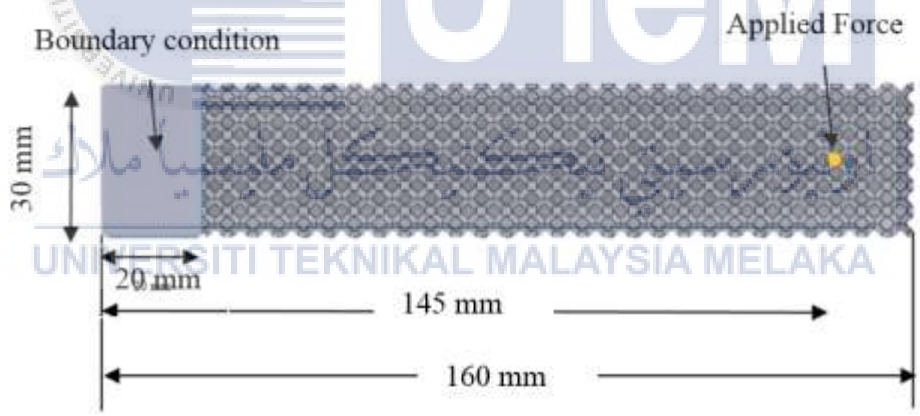

Figure 3.19: Location of excitation point in lattice structure bar (bottom view)

7. Applied the meshing.

- On the Mesh Module is used to generate the finite element mesh. The mesh of the part is created using the element shape and analysis with the standard, 3D stress, C3D10H, is a 10-node quadratic tetrahedron, hybrid, constant pressure.

8. Created and submitted analysis job.

- When the definition of the lattice structure model is complete, an analysis is created and submitted to analyses the model. The job is submitted in the job module and analysis is completed.

9. Viewed the analysis result.

- The result is view in the visualization module.

3.3 Experimental Setup and Procedure

Figure 3.20 illustrated a schematic layout of the experimental system. The diagram shows signal analyzer was connected to the computer through USB 1. An accelerometer that function to detect dynamic sense movement or vibrations and impact hammer are connected to Dataphysics Quattro through channel 4 and channel 3 respectively.

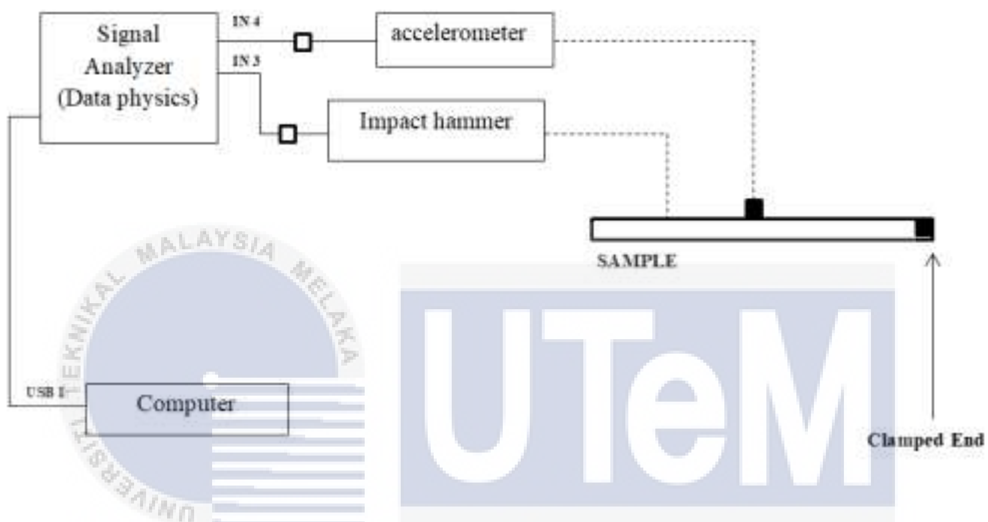

Figure 3.20: Schematic Diagram of the Experimental Setup

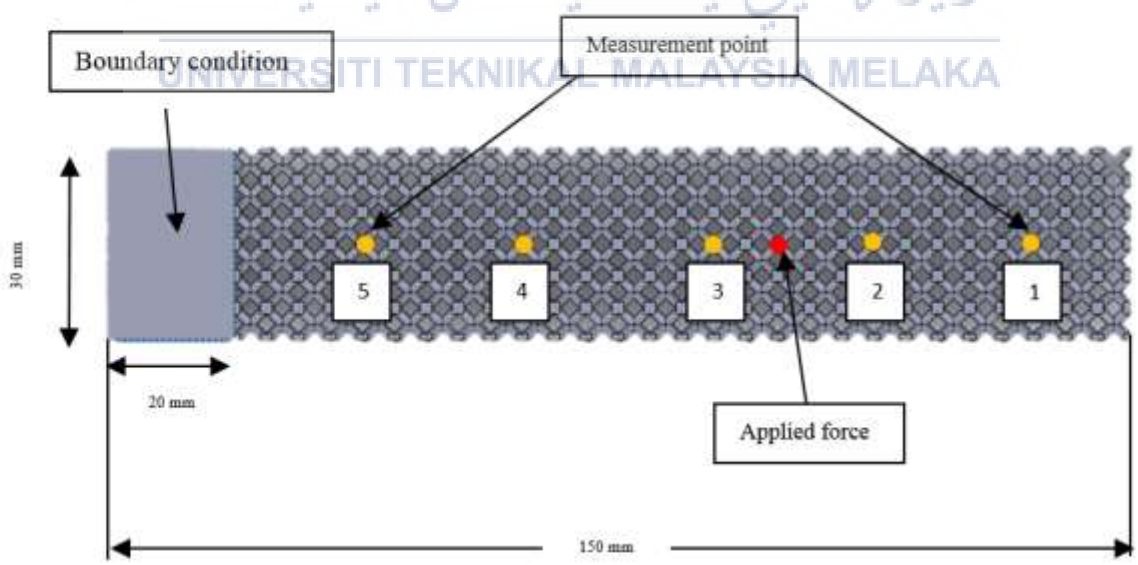

Figure 3.21: Location of measurement point and excitation point

Vibration testing is conducted using four sample which were 1.4 mm, 1.6 mm and 1.8 mm strut size and solid ABS to identify the natural frequencies of all sample. The sample are subjected to boundary condition with one end of the bar clamped-free to the test rig. The location of measurement points and excitation points are shown in Figure. 5. The experimental set up consist of Dataphysics Quattro as signal generator and analyzer, accelerometer and impact hammer. A random force was applied to the sample by using impact hammer. The vibration signal was measured by accelerometer for each measurement points. Data developed from the test were analyzed by using SignalCalc 240 Dynamic Signal Analyzer. The experimental set up for vibration testing is as shown in Figure 3.21. Three readings were taken and averaged for each measurement point for each sample to ensure the consistency of the results measured.

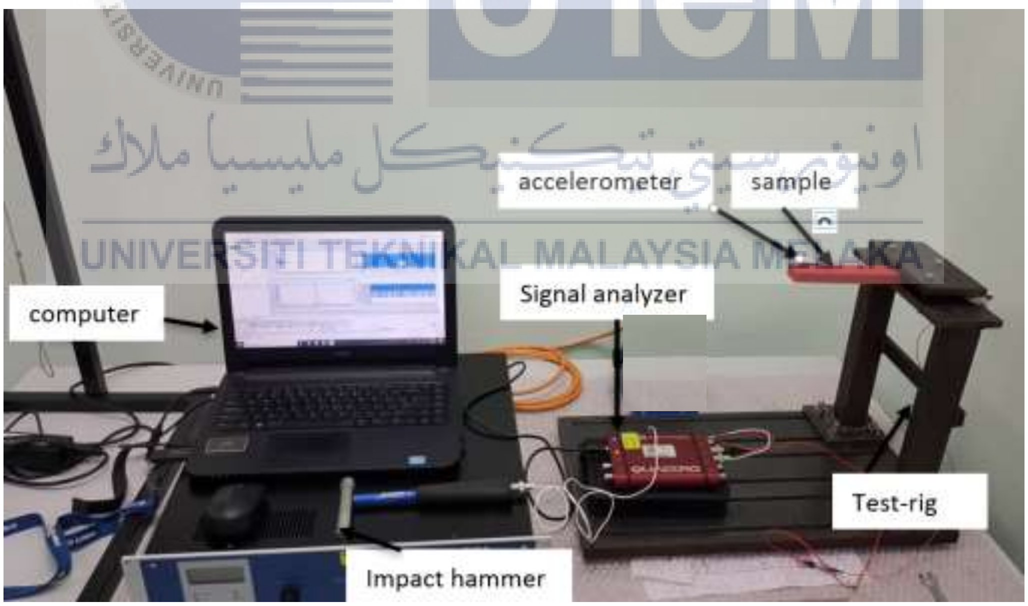

Figure 3.22: Experimental set up for vibration testing

CHAPTER 4

RESULTS AND DISCUSSION

4.1 Overview

In this chapter presents a mesh convergence study conducted to verify the FE models create solutions that have converged to an acceptable limit is presented. Following that, the result of natural frequency for lattice structure and solid structure using FE method are discussed. Next, the stiffness of lattice structure and solid samples of ABS material also discussed here. In addition, for comparison purpose, the natural frequency of lattice structure and solid design of ABS material obtained in the experiment also elaborated here.

The result are divided into four topics which are the convergence study, numerical result, experimental result and comparative study. In numerical result it will be divided into three sub-topics frequency extraction analysis, static analysis and vibration mode shape. Meanwhile, in static analysis the results of sample deflection for ABS lattice is discussed. Next, an experimental result for modal testing conducted of ABS solid bar sample and ABS lattice bar samples with 1.4, 1.6 and 1.8 mm strut diameters is explained. Finally, a comparative study between the FEA result and experimental work is discussed for result validation. Then, the FE method is applied to others materials are also presented.

4.2 Convergence Study

A mesh convergence study was performed to ensure that the FE model produces solutions that have converged to an acceptable limit. The mesh convergence study conducted is to verify the best size of element that appropriate to use in FE models for result on frequency extraction analysis and deflection extraction analysis. The first natural frequency for one-layer lattice structure design of 1.4 mm strut diameter was used as the convergence measurement. Based on the result shown in Table 4.1, the value of natural frequency start to converges at size element 0.49 mm to 0.47 mm. The convergence trend was illustrated in Figure 4.1. The initial size of element chosen was started from 0.52 mm due to the minimum limit of element size suggested by the ABAQUS. If the size element greater than 0.52 mm, poor meshing quality was obtained for FE models. From the result, it can be concluded that the quality of meshing is controlled by the size of element and it was also found that by reducing number of elements also affecting the convergence result.

Table 4.1: Size of element for convergence test

Size of element (mm)	Number of elements	First natural frequency (Hz)
0.52	509143	22.42
0.51	634578	22.41
0.50	637459	22.40
0.49	641116	22.39
0.48	648469	22.39
0.47	650165	22.39

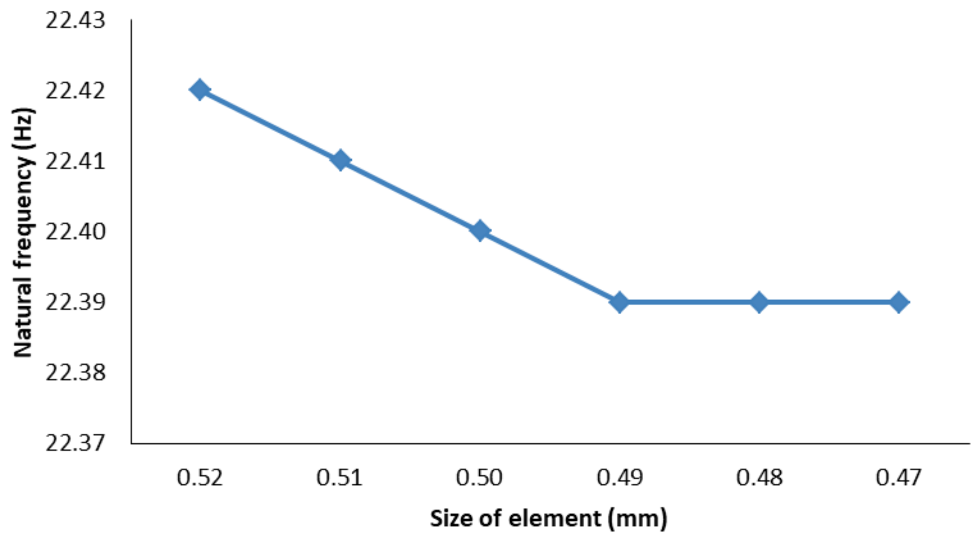

Figure 4.1: Convergence test for FE analysis of ABS lattice structure.

4.3 Numerical Results

The size of element that discussed in mesh convergence study is used in this section to conduct frequency extraction analysis and static analysis. The bar models are discretized using from 524013 to 648653 quadratic solid elements. The number of elements for each bar differs depending on the size of strut diameter. Initially, a frequency extraction analysis is performed using lanczos method to extract the natural frequencies and mode shape of solid and lattice bar models. Then the static deflection analysis is performed to obtain the deflection of the solid and lattice bar models at given force.

4.3.1 Frequency Extraction Analysis

Acrylonitrile butadiene styrene (ABS) is one of the materials used in this study. To perform the analysis some of the material properties need to insert into ABAQUS software such as density, young modulus, and poison ratio as listed in Table 3.1 in previous chapter. The result obtained in Table 4.2 are natural frequency for ABS solid and lattice model, meanwhile Figure 4.2 shows the frequency trend for solid ABS and lattice ABS bar models with different size of strut diameter.

Table 4.2: Frequency extraction analysis for 1st, 2nd, and 3rd modes of vibration for ABS.

FEA Results			
Strut Ø (mm)	**Frequency (Hz)**		
	First vibration mode	**Second vibration mode**	**Third vibration mode**
1.0	41.307	79.383	256.620
1.2	52.126	99.341	321.700
1.4	63.541	120.130	389.600
1.6	75.396	140.020	459.810
1.8	87.673	160.650	533.380
Solid ABS	153.310	247.780	963.600

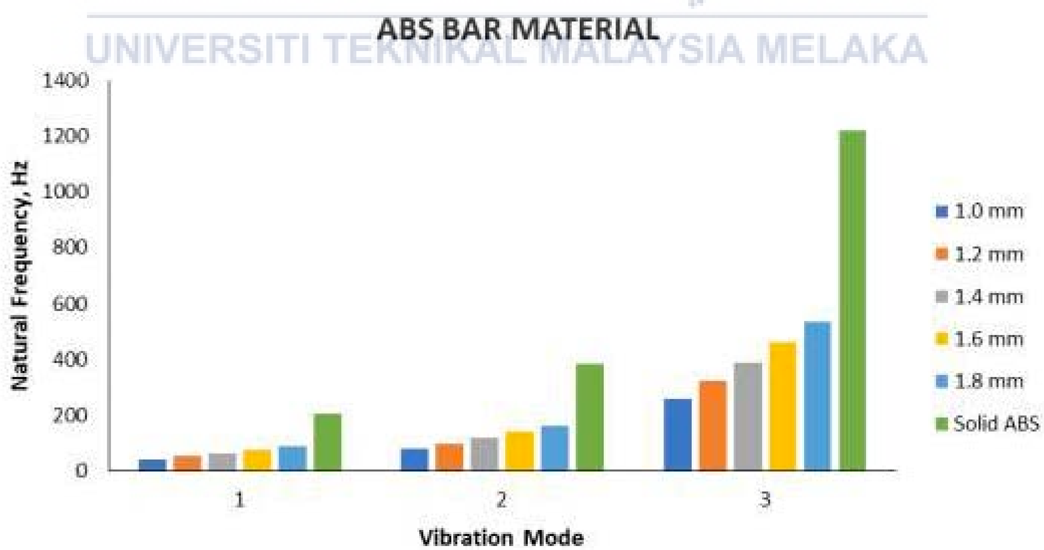

Figure 4.2: The effect of solid bar and lattice bar model strut diameter on natural frequency of ABS.

In Table 4.2 the natural frequency values of ABS obtained from the frequency extraction analysis of the first three modes for solid and lattice bar models are shown. For first, second and third mode of ABS solid bar model has the highest frequency compare to lattice bar models. It can be seen that the large strut diameter for ABS lattice bar models shifts the frequency values of the first, second and third modes upwards, as expected due to increased lattice stiffness. However, the frequency value for ABS solid bar model has the highest frequency compare to ABS lattice bar models due the mass of ABS solid bar much heavy then lattice. This result are also illustrated in Figure 4.2. It shows that the increasing trend of natural frequency for ABS lattice bar models when the size of strut diameter increased. The frequency becoming increased due to the increasing sizes of strut (Azmi et al., 2018). Meanwhile, the highest incrementation in frequency for all three mode of lattice structure found between 1.6 mm and 1.8 mm size of strut were up 13% to 15% frequency increased. By referring Figure 4.2 increasing trend for all three mode and drastically increased between solid and 1.8 mm lattice structure which were up 78% to 80% increased.

4.3.2 Frequency Extraction Conclusion

The influence of the strut diameter of lattice bar models on the frequency response has been observed. It can be seen that, ABS lattice bar model with increase in the strut diameter, the frequency value clearly increases. This is due to increased in lattice stiffness as the diameter become larger which produce highest moment of inertia. However, compared between ABS lattice bar models and ABS solid bar model, the frequency value for solid ABS bar model higher than ABS lattice bar models because ABS solid much stiff than lattice bar. Cannot be considered as lightweight materials because of it weight.

4.3.3 Vibration Mode Shape

This part presents the mode shapes for all FE models. Mode shape is a specific pattern of vibration executed by a mechanical system at a specific frequency. Therefore, different mode shape will be associated with different frequency. The boundary condition considered in the FE models is clamped fixed (CF) to simulate the cantilever beam behavior. The mode shape for the first, second and third vibration mode of the FE models are shown in Table 4.3. From the Table 4.3, it can be seen that the mode shapes obtained for the FE model are similar to the fundamental cantilever beam mode shape.

Table 4.3 show the first three modes of vibration for ABS lattice and ABS solid bar models. The dark blue area in these figures from Table 4.3 indicate nodal displacements for the first three modes of vibration, representing the area where the displacement is close to zero. Meanwhile, the red area show in figure from Table 4.3 are representing the high amplitude for first three modes vibration where the displacement are maximum and close to one.

Table 4.3: The first three vibration mode shapes of lattice structure and solid design

Strut Ø (mm)	**Vibration mode shapes of solid and lattice structure design**		
	first mode	**Second mode**	**Third mode**
1.0	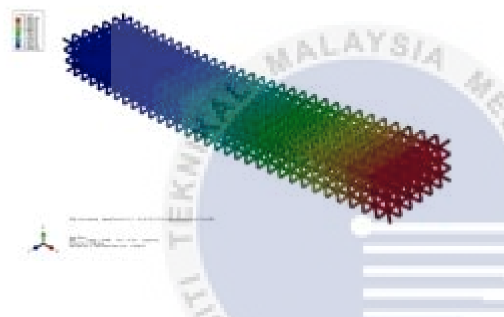	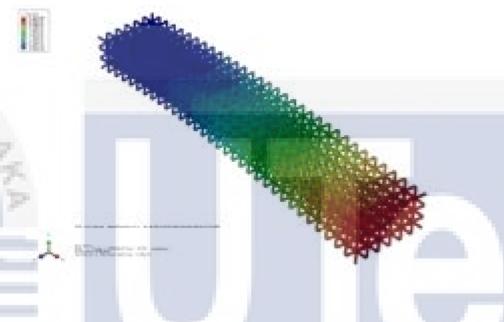	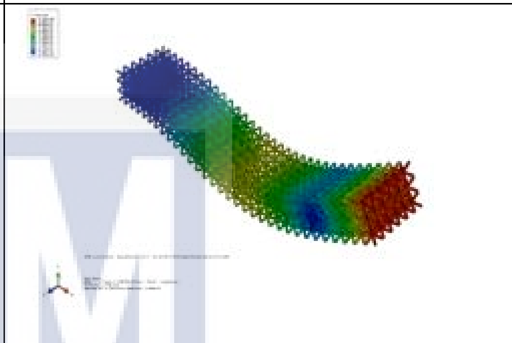
1.2	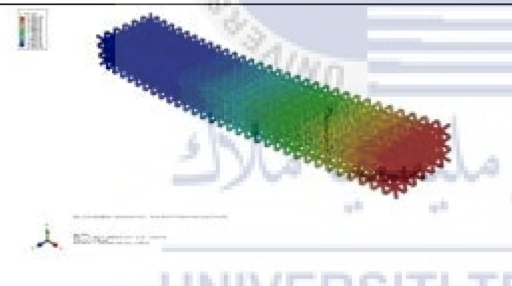	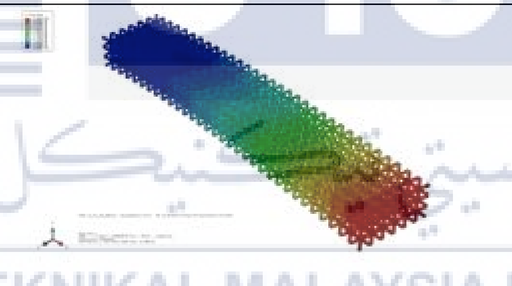	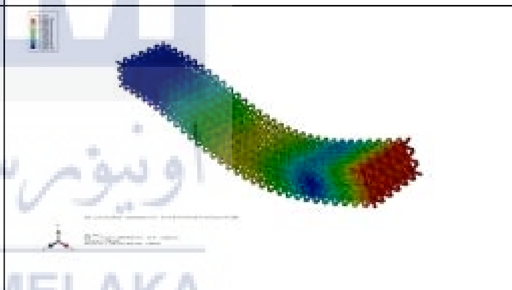

Strut Ø (mm)	Vibration mode shapes of solid and lattice structure design		
	First mode	**Second mode**	**Third mode**
1.4	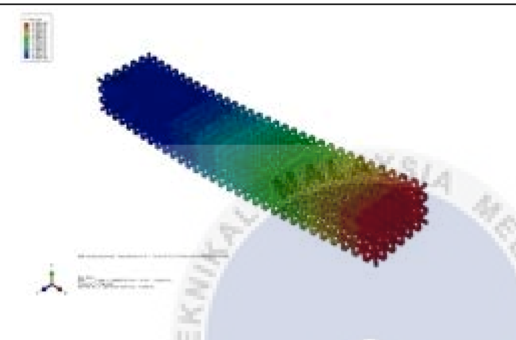	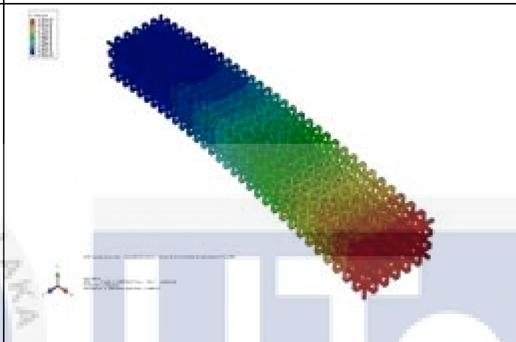	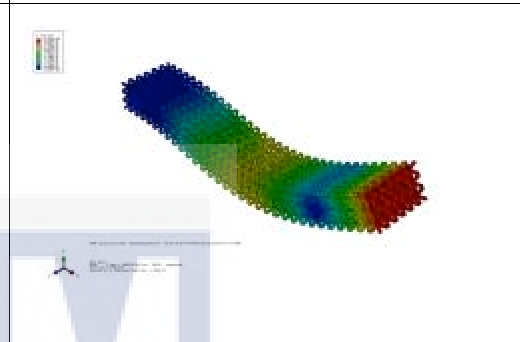
1.6	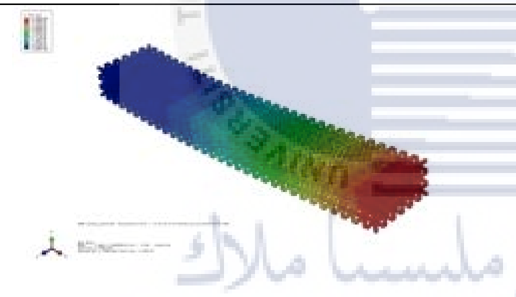	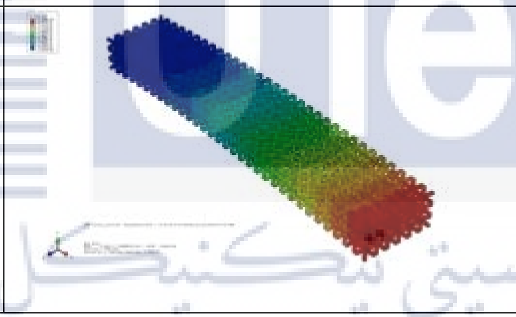	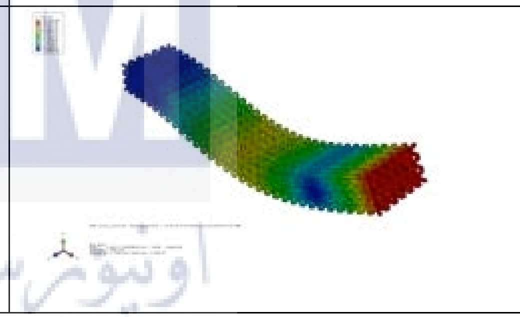

Strut Ø (mm)	Vibration mode shapes of solid and lattice structure design		
	First mode	Second mode	Third mode
1.8	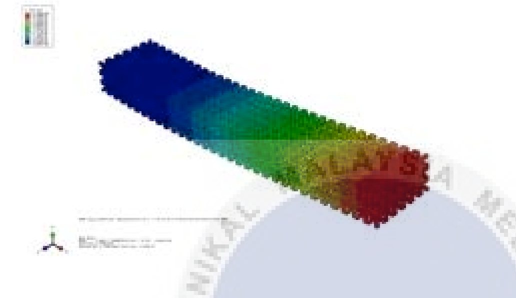	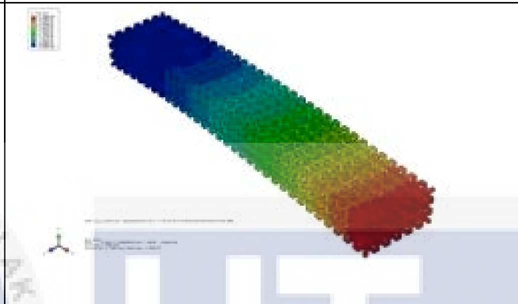	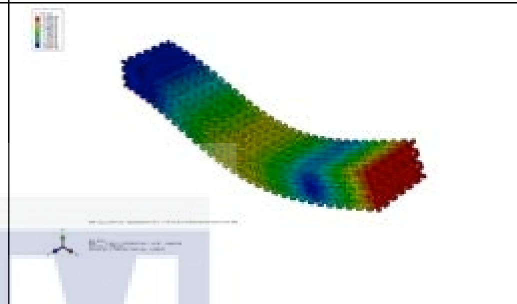
Solid	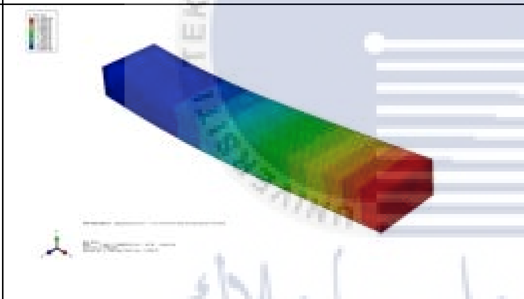	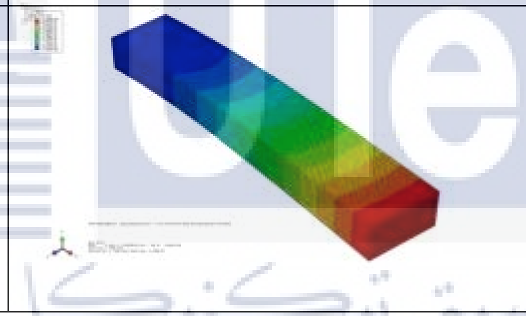	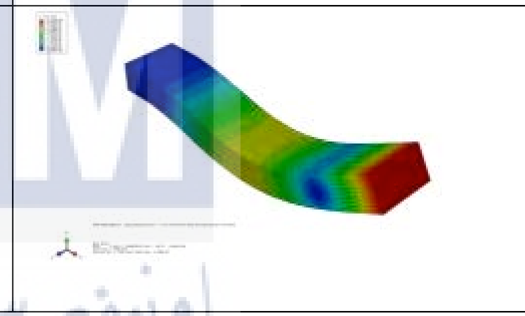

4.3.3 Static Analysis of ABS Lattice And ABS Solid Bar Model.

To prove the frequency extraction analysis that conducted from previous section, static analysis to calculate the stiffness in each model was conducted. The effect of strut diameter of ABS lattice bar model and ABS solid bar model on stiffness value are conducted. The result obtain was tabulated in Table 4.5 ABS solid, meanwhile Table 4.6 to Table 4.10 shows the result for 1.0mm, 1.2mm, 1.4mm, 1.6mm and 1.8 mm strut diameter, respectively. Figure 4.3 show trend of stiffness for lattice and solid ABS bar model and Table 4.4 show the maximum deflection according the maximum force applied in FE model during analysis.

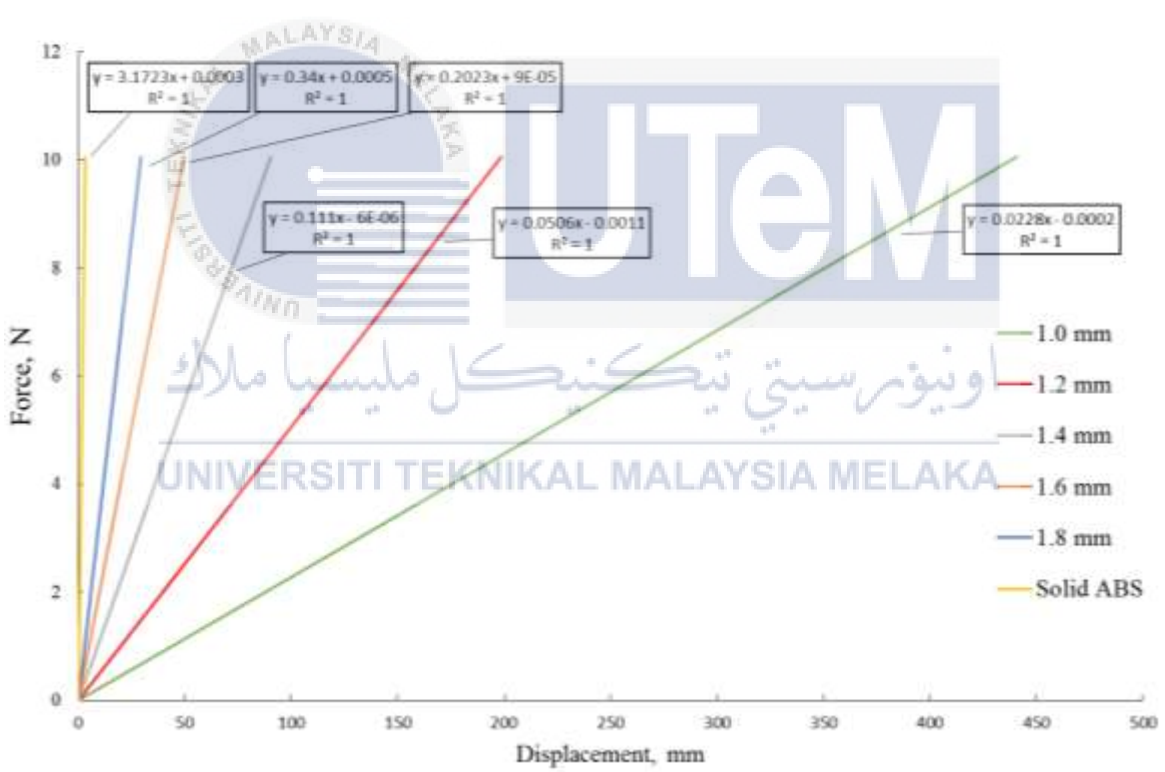

Figure 4.3: The relation force and deflection to the stiffness.

Table 4.4: Maximum force and deflection

Design	Maximum Force, F (N)	Maximum Deflection, *x* (m)	Stiffness, *k* (N/m)
Solid ABS	10.0	3.152×10^{-4}	31.70×10^{3}
1.0 mm	10.0	3.152×10^{-4}	2.28×10^{2}
1.2 mm	10.0	1.978×10^{-2}	5.06×10^{2}
1.4 mm	10.0	4.383×10^{-2}	1.11×10^{3}
1.6 mm	10.0	4.944×10^{-3}	2.02×10^{3}
1.8 mm	10.0	2.941×10^{-3}	3.40×10^{3}

The maximum force applied and deflection that obtain from the analysis shown in Table 4.4. Solid ABS bar models show the highest stiffness with 31.7 kN/m. For lattice structure design the stiffness is different due to the different size of strut diameter where the higher stiffness shown in 1.8 mm strut size which is 3.40 kN/m. Next, the 1.0 mm strut diameter size shows the lower stiffness with 0.228 kN/m. Following that, the stiffness of 1.2 mm, 1.4 mm, 1.6 mm strut size is 0.506 kN/m, 1.11 kN/m and 2.02 kN/m respectively. The stiffness increase when the size of diameter strut was increase. From data tabulated in Table 4.6, ABS solid has higher stiffness compared to ABS lattice structure bar because ABS solid bar have higher cross-sectional area and total moment inertia compared to lattice structure design. The increasing of stiffness is due to the increasing of cross-sectional area that effect the total moment of inertia where directly will affect the stiffness (Azmi et al., 2018).

Table 4.5: The stiffness of solid ABS bar model.

Force, F (N)	Deflection, x (m)	Stiffness, k (N/m)
1.0	3.152×10^{-5}	31.7×10^{3}
1.5	4.728×10^{-5}	31.7×10^{3}
2.0	6.304×10^{-5}	31.7×10^{3}
2.5	7.880×10^{-5}	31.7×10^{3}
3.0	9.456×10^{-5}	31.7×10^{3}
3.5	1.103×10^{-4}	31.7×10^{3}
4.0	1.261×10^{-4}	31.7×10^{3}
4.5	1.418×10^{-4}	31.7×10^{3}
5.0	1.576×10^{-4}	31.7×10^{3}
5.5	1.734×10^{-4}	31.7×10^{3}
6.0	1.891×10^{-4}	31.7×10^{3}
6.5	2.049×10^{-4}	31.7×10^{3}
7.0	2.207×10^{-4}	31.7×10^{3}
7.5	2.364×10^{-4}	31.7×10^{3}
8.0	2.522×10^{-4}	31.7×10^{3}
8.5	2.679×10^{-4}	31.7×10^{3}
9.0	2.837×10^{-4}	31.7×10^{3}
9.5	2.995×10^{-4}	31.7×10^{3}
10.0	3.152×10^{-4}	31.7×10^{3}

Table 4.6: The stiffness of 1.0 mm strut diameter lattice ABS bar model.

Force, F (N)	Deflection, x (m)	Stiffness, k (N/m)
1.0	3.152×10^{-5}	2.28×10^{2}
1.5	4.728×10^{-5}	2.28×10^{2}
2.0	6.304×10^{-5}	2.28×10^{2}
2.5	7.880×10^{-5}	2.28×10^{2}
3.0	9.456×10^{-5}	2.28×10^{2}
3.5	1.103×10^{-4}	2.28×10^{2}
4.0	1.261×10^{-4}	2.28×10^{2}
4.5	1.418×10^{-4}	2.28×10^{2}
5.0	1.576×10^{-4}	2.28×10^{2}
5.5	1.734×10^{-4}	2.28×10^{2}
6.0	1.891×10^{-4}	2.28×10^{2}
6.5	2.049×10^{-4}	2.28×10^{2}
7.0	2.207×10^{-4}	2.28×10^{2}
7.5	2.364×10^{-4}	2.28×10^{2}
8.0	2.522×10^{-4}	2.28×10^{2}
8.5	2.679×10^{-4}	2.28×10^{2}
9.0	2.837×10^{-4}	2.28×10^{2}
9.5	2.995×10^{-4}	2.28×10^{2}
10.0	3.152×10^{-4}	2.28×10^{2}

Table 4.7: The stiffness of 1.2 mm strut diameter lattice ABS bar model.

Force, F (N)	**Deflection, *x* (m)**	**Stiffness, *k* (N/m)**
1.0	1.978×10^{-3}	5.06×10^{2}
1.5	2.267×10^{-3}	5.06×10^{2}
2.0	3.956×10^{-3}	5.06×10^{2}
2.5	4.945×10^{-3}	5.06×10^{2}
3.0	5.934×10^{-3}	5.06×10^{2}
3.5	6.923×10^{-3}	5.06×10^{2}
4.0	7.912×10^{-3}	5.06×10^{2}
4.5	8.900×10^{-3}	5.06×10^{2}
5.0	9.889×10^{-3}	5.06×10^{2}
5.5	1.088×10^{-2}	5.06×10^{2}
6.0	1.187×10^{-2}	5.06×10^{2}
6.5	1.286×10^{-2}	5.06×10^{2}
7.0	1.385×10^{-2}	5.06×10^{2}
7.5	1.483×10^{-2}	5.06×10^{2}
8.0	1.582×10^{-2}	5.06×10^{2}
8.5	1.681×10^{-2}	5.06×10^{2}
9.0	1.780×10^{-2}	5.06×10^{2}
9.5	1.879×10^{-2}	5.06×10^{2}
10.0	1.978×10^{-2}	5.06×10^{2}

Table 4.8: The stiffness of 1.4 mm strut diameter lattice ABS bar model.

Force, F (N)	Deflection, x (m)	Stiffness, k (N/m)
1.0	4.383×10^{-3}	1.11×10^{3}
1.5	6.574×10^{-3}	1.11×10^{3}
2.0	8.765×10^{-3}	1.11×10^{3}
2.5	1.096×10^{-2}	1.11×10^{3}
3.0	1.315×10^{-2}	1.11×10^{3}
3.5	1.534×10^{-2}	1.11×10^{3}
4.0	1.753×10^{-2}	1.11×10^{3}
4.5	1.972×10^{-2}	1.11×10^{3}
5.0	2.191×10^{-2}	1.11×10^{3}
5.5	2.410×10^{-2}	1.11×10^{3}
6.0	2.630×10^{-2}	1.11×10^{3}
6.5	2.849×10^{-2}	1.11×10^{3}
7.0	3.068×10^{-2}	1.11×10^{3}
7.5	3.287×10^{-2}	1.11×10^{3}
8.0	3.506×10^{-2}	1.11×10^{3}
8.5	3.725×10^{-2}	1.11×10^{3}
9.0	3.944×10^{-2}	1.11×10^{3}
9.5	4.163×10^{-2}	1.11×10^{3}
10.0	4.383×10^{-2}	1.11×10^{3}

Table 4.9: The stiffness of 1.6 mm strut diameter lattice ABS bar model.

Force, F (N)	**Deflection, *x* (m)**	**Stiffness, *k* (N/m)**
1.0	4.944×10^{-4}	2.02×10^{3}
1.5	7.416×10^{-4}	2.02×10^{3}
2.0	9.888×10^{-4}	2.02×10^{3}
2.5	1.236×10^{-3}	2.02×10^{3}
3.0	1.483×10^{-3}	2.02×10^{3}
3.5	1.730×10^{-3}	2.02×10^{3}
4.0	1.978×10^{-3}	2.02×10^{3}
4.5	2.225×10^{-3}	2.02×10^{3}
5.0	2.472×10^{-3}	2.02×10^{3}
5.5	2.719×10^{-3}	2.02×10^{3}
6.0	2.966×10^{-3}	2.02×10^{3}
6.5	3.214×10^{-3}	2.02×10^{3}
7.0	3.461×10^{-3}	2.02×10^{3}
7.5	3.708×10^{-3}	2.02×10^{3}
8.0	3.955×10^{-3}	2.02×10^{3}
8.5	4.202×10^{-3}	2.02×10^{3}
9.0	4.450×10^{-3}	2.02×10^{3}
9.5	4.697×10^{-3}	2.02×10^{3}
10.0	4.944×10^{-3}	2.02×10^{3}

Table 4.10: The stiffness of 1.8 mm strut diameter lattice ABS bar model.

Force, F (N)	**Deflection, *x* (m)**	**Stiffness, *k* (N/m)**
1.0	2.941×10^{-4}	3.4×10^{3}
1.5	4.411×10^{-4}	3.4×10^{3}
2.0	5.882×10^{-4}	3.4×10^{3}
2.5	7.352×10^{-4}	3.4×10^{3}
3.0	8.823×10^{-4}	3.4×10^{3}
3.5	1.029×10^{-3}	3.4×10^{3}
4.0	1.176×10^{-3}	3.4×10^{3}
4.5	1.323×10^{-3}	3.4×10^{3}
5.0	1.470×10^{-3}	3.4×10^{3}
5.5	1.618×10^{-3}	3.4×10^{3}
6.0	1.765×10^{-3}	3.4×10^{3}
6.5	1.912×10^{-3}	3.4×10^{3}
7.0	2.059×10^{-3}	3.4×10^{3}
7.5	2.206×10^{-3}	3.4×10^{3}
8.0	2.353×10^{-3}	3.4×10^{3}
8.5	2.500×10^{-3}	3.4×10^{3}
9.0	2.647×10^{-3}	3.4×10^{3}
9.5	2.794×10^{-3}	3.4×10^{3}
10.0	2.941×10^{-3}	3.4×10^{3}

4.4 Experimental Result

This section presents an experimental study of the dynamics of the ABS bar sample which include ABS lattice bar and ABS solid bar. Experimental measurement fundamental natural frequency values are carried out, and then compared with finite element (FE) results in order to verify the FE model.

Table 4.11: Experimental results for the first and second modes of vibration for ABS.

Strut Ø (mm)	First vibration mode frequency, Hz	
	1st	2nd
1.4 mm	53.00	312.00
1.6 mm	68.00	413.00
1.8 mm	82.00	506.00
Solid ABS	159.00	1000.00

Table 4.11 show the results obtained from the tests. It can be seen that the frequency increases with the increasing the size of strut diameter for ABS lattice bar, for all two modes of vibration. The frequencies of the first mode vibration of the ABS lattice bar samples obtained were 53.00,68.00 and 82.00 Hz for the 1.4, 1.6 and 1.8 mm strut diameter size, respectively, while for ABS solid bar sample the frequency obtained was 159.00 Hz. In term of strut diameter size, the same phenomenon was encountered as in finite element (FE) analysis, whereby the frequency increase when the size of strut diameter increase. However, for ABS solid bar sample the frequency value obtained was higher than ABS lattice bar. This is due to the ABS solid bar sample much stiff and heavy compared to ABS lattice sample as shown in the result obtained in previous section.

(a)

(b)

(c)

(d)

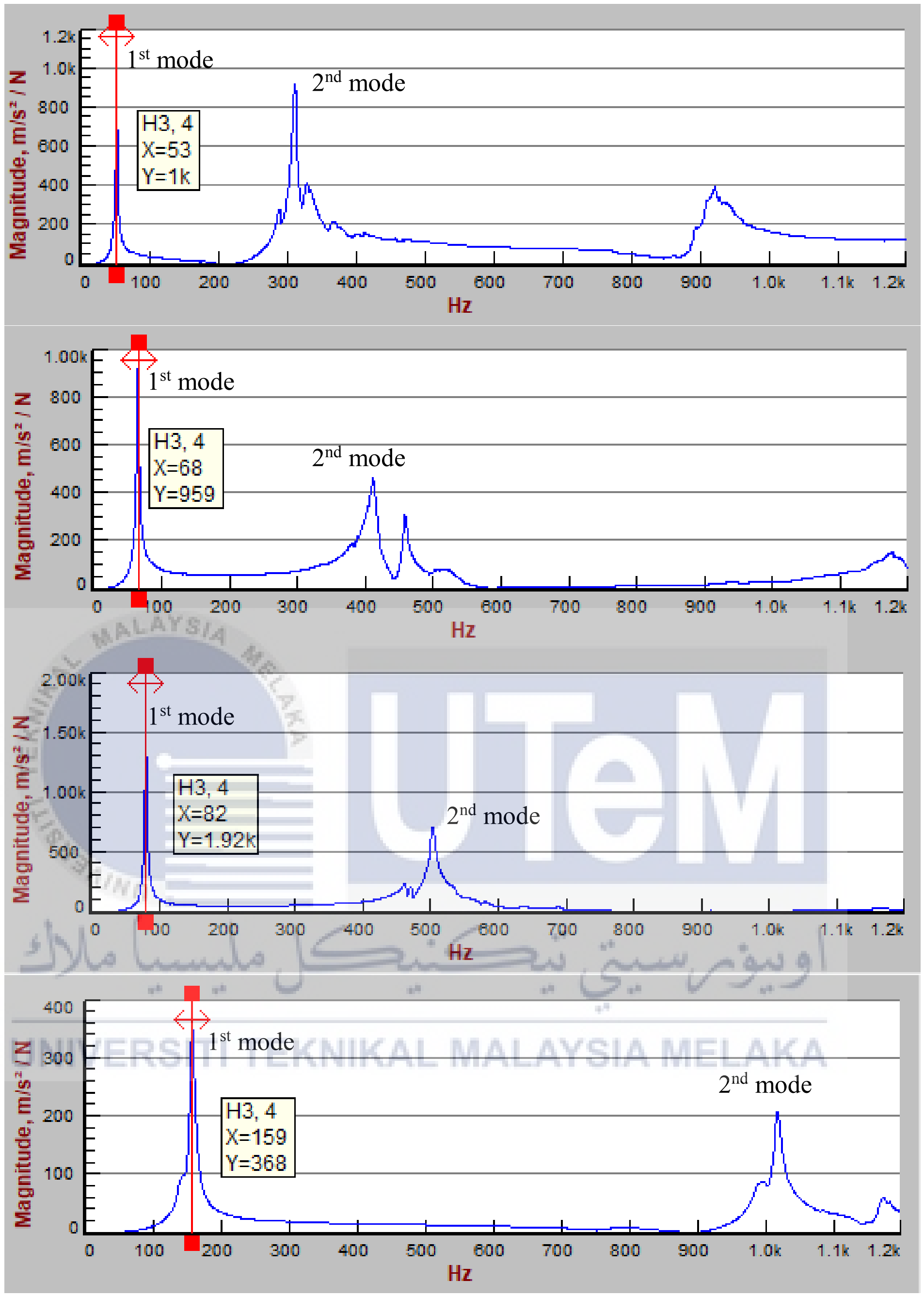

Figure 4 4: Frequency response first two vibration modes (a) 1.4 mm, (b) 1.6 mm, (c) 1.8 mm, and (d) Solid ABS

4.5 Comparative Study and Discussion

4.5.1 Comparison between Finite Element Method and Experimental Method

The comparative study of the numerical approaches with experimental measurement are carried out for verification of the study. The result in this study was tabulated in Table 4.12 below.

Table 4.12: Comparison of natural frequency for the finite element analysis and experimental work for 1st mode only.

Strut Ø (mm)	First Mode of Natural Frequency, Hz		Error (%)
	Finite Element (FE)	Experimental	
1.4	63.54	53.00	16.59
1.6	75.39	68.00	9.80
1.8	87.67	82.00	6.48
Solid ABS	153.31	159.00	3.71

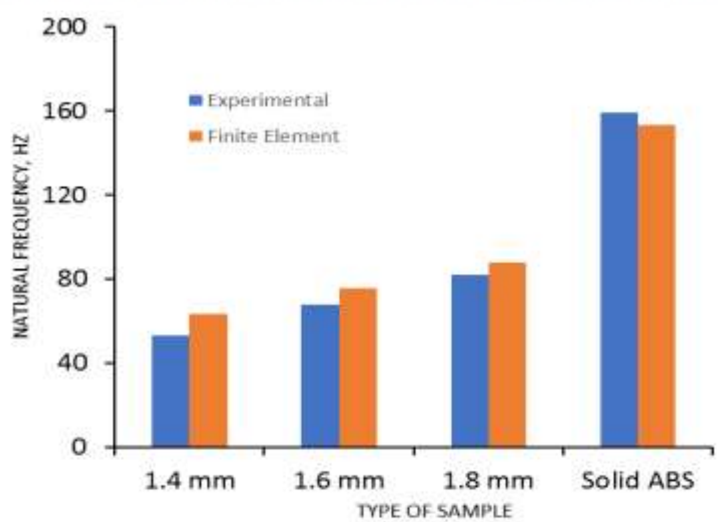

Figure 4.5: Comparisons of the experimental and numerical results of the natural frequencies.

The 1st mode natural frequency values from the FE analysis and experimental work of the ABS lattice and solid ABS are presented in Table 4.12. The percentage error between the two values, with respect to the FE result, is shown in the fourth column. From the result, it can be seen that the percentage error is less than 17% for all design with the highest error shown by the strut diameter 1.4 mm design, while the lowest percentage error of 3.71% shown by solid ABS design. It is clear that the FE model accurately predicts the natural frequencies of the bar sample. There is good agreement between the experimental and FE values for the ABS lattice bar model natural frequency with a difference value of just 3.71%.

4.5.2 Comparison between ABS, Titanium and Stainless-Steel Materials

From the results obtained, the comparison between FE and experimental method for ABS material for both ABS solid and lattice bar model shows a very good agreement, thus the comparison using FE method between ABS materials with other materials which were titanium and stainless-steel was conducted. The comparison only made between ABS with titanium and stainless-steel using FE method. The titanium and stainless-steel materials are powder-based material and can only be printed using SLS or SLM 3D printing Additive manufacturing (AM) printer. As known the time duration and cost to print the sample are long and much more expensive compared to ABS material. Thus, finite element (FE) method is one of the best solution to analyze product from these types of material to understand their behavior. The frequency extraction analysis for titanium and stainless-steel is conducted using the validated FE method and the result is presented in this section.

Titanium inherits an array of the outstanding properties of dense titanium materials such as high specific strength, stiffness, excellent corrosion resistance, and biocompatibility

(Tang et al., 2015). The first three natural frequency of titanium was tabulated in Table 4.13. Next, Figure 4.3 shows the trend of natural frequency of titanium lattice and titanium solid models.

Table 4.13: Frequency extraction analysis for 1st, 2nd, and 3rd modes of vibration for Titanium.

FEA Results			
Strut Ø (mm)	**Frequency (Hz)**		
	First vibration mode	**Second vibration mode**	**Third vibration mode**
1.0	123.55	237.42	767.61
1.2	155.88	297.05	962.12
1.4	189.98	359.18	1165.00
1.6	225.48	418.87	1375.30
1.8	262.52	480.78	1595.70
Solid Titanium	610.09	1144.10	3652.80

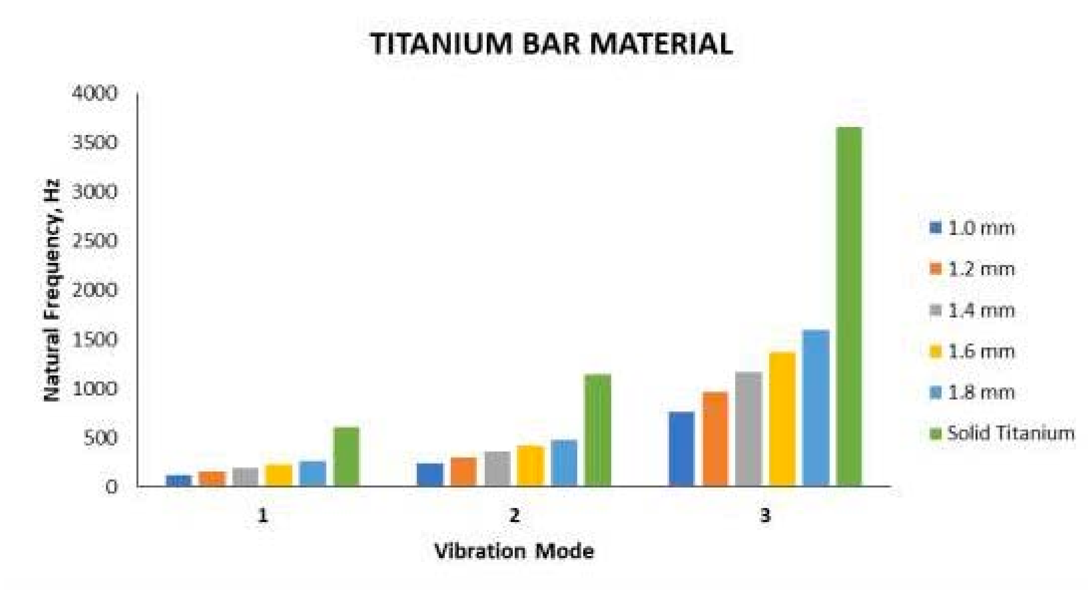

Figure 4.6: The effect of solid and lattice structure strut diameter on natural frequency of titanium.

For solid and lattice bar models, the natural frequency values of titanium material taken from the frequency extraction analysis are shown in Table 4.13. First, second and third modes of titanium solid bar model have the highest frequency compared to models of titanium lattice bars. The large strut diameter for titanium lattice bar models can be seen to shift the frequency values of the first, second and third modes upwards as expected due to increased lattice stiffness. However, due to the mass of titanium solid bar heavy then lattice, the frequency value for solid titanium bar model has the highest frequency compared to titanium lattice bar models. This result is also illustrated in Figure 4.6 shows that when the lattice strut diameter increased the increasing trend of natural frequency for lattice titanium bar models. The phenomenon that happened in ABS material are similar happened in titanium where the frequency increased when the size of strut diameter increased. The value of frequency is depending on the size of strut diameter (Azmi et al., 2017). Besides that, from Figure 4.6 shown the significant increase in 1.0 mm to 1.8 mm lattice bar models and increase dramatically between lattice bar models and solid bar model design which is 79% ,81% and 78% in first, second and third mode respectively.

Finally, the stainless steel was used to make comparison with ABS and titanium for frequency extraction analysis. The first, second and third mode of natural frequency from stainless steel for lattice structure and solid design are shown in Table 4.14 and Figure 4.7 show the natural frequency extraction trend for lattice and solid bar models for stainless steel.

Table 4.14: Frequency extraction analysis for 1st, 2nd, and 3rd modes of vibration for stainless steel.

FEA Results			
Strut Ø (mm)	**Frequency (Hz)**		
	First vibration mode	**Second vibration mode**	**Third vibration mode**
1.0 mm	118.62	227.88	737.05
1.2 mm	149.57	284.99	937.05
1.4 mm	182.21	344.54	1117.80
1.6 mm	216.42	402.32	1320.60
1.8 mm	252.14	462.32	1533.20
Solid 316SS	589.22	1106.50	3531.70

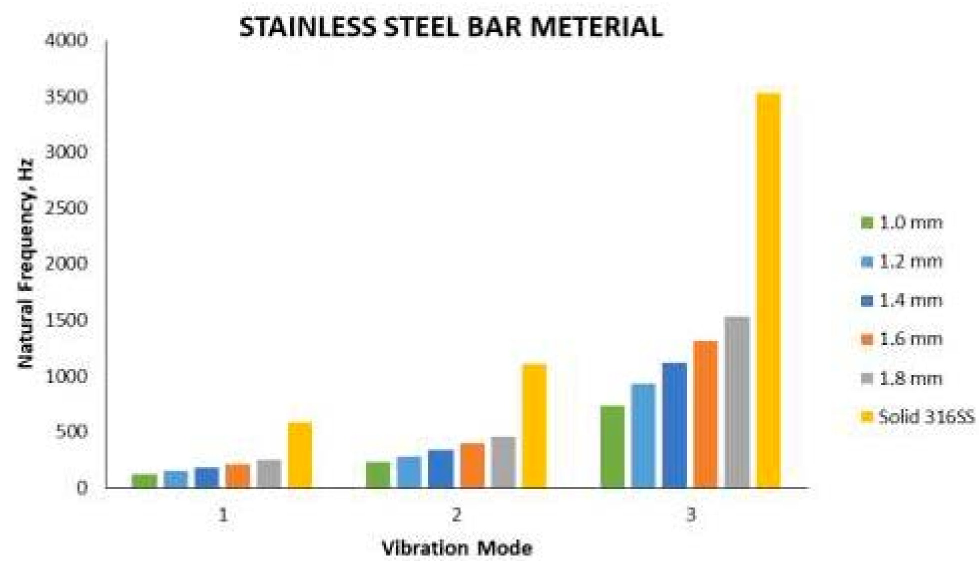

Figure 4.7: The effect of solid bar and lattice strut diameter on natural frequency of stainless steel.

In this section the same phenomenon was encountered as in previous material (ABS and Titanium). The natural frequency values of ABS taken from the frequency extraction analysis of the first three modes are shown in Table 4.14 for stainless-steel solid bar model and stainless-steel lattice bar models. First, second and third modes of stainless-steel solid bar model have the highest frequency compared to stainless-steel lattice bar models. The large strut diameter for lattice bar models can be seen shifting the frequency values of the first, second and third modes upwards as predictable due to increased lattice stiffness. However, due to the mass of stainless-steel solid bar much heavy then stainless-steel lattice structure, the frequency value for solid bar model has the highest frequency compared to lattice bar models. The relation between natural frequency and strut size are directly proportional which were increased strut size can increase natural frequency (Azmi et al., 2018). Meanwhile, the frequency increased from lattice models to solid model which were 79% to 81% increased.

From the comparison frequency extraction between ABS, titanium and stainless-steel. It shows natural frequency obtained for titanium shows the higher frequency compared to ABS and stainless-steel. The frequency is higher obtained from titanium and stainless-steel compare to ABS due to higher modulus of elasticity which were 114 GPa and 193 GPa for titanium and stainless-steel respectively and 3 GPa for ABS. Altintas said when the modulus of elasticity increased, the natural frequency also increased. From the Figure 4.6 and Figure 4.7, it shown the trend of titanium and stainless-steel materials are similar with ABS material where the size of strut diameter was affecting the natural frequency. The higher size of strut diameter of lattice bar model the higher natural frequency obtained.

CHAPTER 5

CONCLUSION AND RECOMMENDATION

5.1 Overview

This chapter present the conclusion of the study where concluded from the objectives of study. Next, the recommendation for further study also suggested in this chapter.

5.2 Conclusion

This study present the results of the vibration characteristic for static and dynamics analysis using finite element (FE) method of solid and lattice bar model for ABS material. It shows the size of strut diameter was affected the natural frequency value of ABS lattice bar models, large strut diameter for ABS lattice bar models shifts the frequency values of the first, second and third modes upwards, as expected due to increased lattice stiffness. However, the frequency value for ABS solid bar model has the highest frequency compare to ABS lattice bar models due the mass of ABS solid bar much heavy then lattice. In static analysis, the effect of size strut diameter to the stiffness of ABS lattice models, as expected the larger strut diameter of ABS lattice models is stiffer due to the larger cross-sectional area that effect the total moment of inertia. Nevertheless, the ABS solid bar model is more stiff compared to ABS lattice models due to high cross-sectional area and total moment of inertia.

Moreover, the experimental measurement of vibration testing for fundamental natural frequencies value using ABS solid bar sample and ABS lattice bar samples show the same phenomena happen in FE method for dynamic analysis. The natural frequency of ABS lattice sample was affected by the size strut diameter. The natural frequency for ABS solid bar sample is much higher compared to ABS lattice bar sample due to the mass of ABS solid bar much heavy. However, due to an increasing implementation of lightweight structures in various application especially in aerospace and automotive industries, lattice structure is most suitable to fulfill demand

Finally, the comparison study between experimental work and FE method has observed. The natural frequency for first vibration shows good agreement with error less than 17%. Using the validated FE method, the frequency extraction analysis was observed using different type of materials which were titanium and stainless steel. The frequency is higher obtained from titanium and stainless-steel compare to ABS due to higher modulus of elasticity. Altintas said when the modulus of elasticity increased, the natural frequency also increased. It also shows the influence of size diameter strut to both material lattice natural frequency. As expected, the same phenomena encountered with ABS material.

5.3 Recommendation

For further study, the study of vibration behavior can be conduct with using the different types of topological lattice structure design. In addition, the experimental worked can be conduct by printing the sample using the other type of additive manufacturing (AM) method for titanium and stainless-steel.

REFERENCES

Abdollah, M. F., & Hassan, R. (2013). Preliminary design of side door impact beam for passenger cars using aluminium alloy. Journal of Mechanical Engineering and Technology, 5(1), 11–18. Retrieved from http://journal.utem.edu.my/index.php/jmet/article/view/316/201.

Altıntas, Gökhan. "Effect of material properties on vibrations of nonsymmetrical axially loaded thin-walled Euler-Bernoulli beams." Mathematical and Computational Applications 15.1 (2010): 96-107.

Alsalla H , Hao L , Smith C . Fracture toughness and tensile strength of 316 L stain- less steel cellular lattice structures manufactured using the selective laser melting technique. Mater Sci Eng: A 2016;669:1–6 7/4/ .

Ashby, M. 2013. Designing architectured materials. Scripta Materialia, 68(1):4{7.

Ashby, M. F., T. Evans, N. A. Fleck, J. Hutchinson, H. Wadley, and L. Gibson 2000. *Metal Foams: A Design Guide*. Elsevier.

Ashby, M. 2006. The properties of foams and lattices. Philosophical Transactions of the Royal Society of London A: Mathematical, Physical and Engineering Sciences, 364(1838):15{30

Azman, A. H. (2017). Method for integration of lattice structures in design for additive manufacturing (Doctoral dissertation, Université Grenoble Alpes).

Azmi, M.S., Hasan R., Ismail, R., Rosli, N.A. and Alkahari, M.R. (2018) ‘Static and dynamic analysis of FDM printed lattice structures for sustainable lightweight material application’, Progress in Industrial Ecology – An International Journal, Vol. 12, No. 3, pp.247-259,

Brennan-Craddock, J., Brackett, D., Wildman, R., & Hague, R. (2012). The design of impact absorbing structures for additive manufacture. *Journal of Physics: Conference Series*, *382*(1). https://doi.org/10.1088/1742-6596/382/1/012042

Budynas, R. G., & Nisbett, J. K. (2011). Shigley's Mechanical Engineering Design (p. 954-955). New York: McGrawHill.

Burlayenko, V. N., Altenbach, H., & Sadowski, T. (2015). An evaluation of displacement-based finite element models used for free vibration analysis of homogeneous and composite plates. Journal of Sound and Vibration, 358, 152–175.

Clevenson, S. A., Dempsey, T. K., & Leatherwood, J. D. (1978). Effect of Vibration Duration on Human Discomfort NASA Technical Paper 1283 Effect of Vibration Duration on Human Discomfort, (September).

Cook, Robert D., Malkus, David S., Concepts and Applications of Finite Element Analysis. John Wiley & Sons, 2007.

Crupi, V., Kara, E., Epasto, G., Guglielmino, E., and Aykul, H. (2017) ‘Static behavior of lattice structures produced via direct metal laser sintering technology’, *Materials & Design*, Vol. 135, pp. 246-256.

Dong, L., V. Deshpande, and H. Wadley 2015. Mechanical response of ti{6al{4v octet-truss lattice structures. *International Journal of Solids and Structures*, 60:107{124

Dong, X. J., Meng, G., Li, H. G., & Ye, L. (2005). Vibration analysis of a stepped laminated composite Timoshenko beam. Mechanics Research Communications, 32(5), 572–581.

Elmadih, Waiel A. and Syam, Wahyudin P. and Maskery, Ian and Leach, Richard (2017) Additively manufactired lattice structures for precision engineering applications. In: 32nd Annual Meeting of the American Society for Precision Engineering, October 29 – November 3, 2017, Charlotte, North Carolina, USA.

Evans, A. G., J. W. Hutchinson, N. A. Fleck, M. Ashby, and H. Wadley 2001. The topological design of multifunctional cellular metals. Progress in Materials Science, 46(3):309{327.

Gibson, L. J. and M. F. Ashby 1999. Cellular solids: structure and properties. Cambridge university press.

Gibson, L. J. 2005. Biomechanics of cellular solids. Journal of biomechanics, 38(3):377{ 399.

Gibson L , Ashby M , Schajer G , Robertson C . The mechanics of two-dimensional cel- lular materials. Proc R Soc Lond A: Math Phys Eng Sci 1982;382(1782):25–42 The Royal Society .

Gibson LJ , Ashby MF . The mechanics of three-dimensional cellular materials. Proc R Soc Lond A: Math Phys Eng Sci 1982;382(1782):43–59 The Royal Society .

Hadi, A., Vignat, F., & Villeneuve, F. (2015, March). Design configurations and creation of lattice structures for metallic additive manufacturing. In 14ème Colloque National AIP PRIMECA.

Hasan, R., Mines, R. A., Shen, E., Tsopanos, S., and Cantwell, W. (2011) 'Comparison on compressive behaviour of aluminium honeycomb and titanium alloy micro lattice blocks', Key Engineering Materials, Vol. 462, pp. 213-218.

Ismail, Rainah (2013) Vibration analysis of a plate with an arbitrarily orientated surface crack. PhD thesis. Retrieved from http://theses.gla.ac.uk/4002/

Jamshidinia M , Wang L , Tong W , Ajlouni R , Kovacevic R . Fatigue properties of a dental implant produced by electron beam melting (EBM). J Mater Process Technol 2015;226:255–63

J. C. Wallach and L. J. Gibson, "Mechanical behavior of a three-dimensional truss material," International Journal of Solids and Structures, vol. 38(pp. 7181-7196, 2000.

Jen, M. U., & Magrab, E. B. (1993). Natural Frequencies and Mode Shapes of Beams Carrying a Two Degree-of-Freedom Spring-Mass System. Journal of Vibration and Acoustics, 115(2), 202. doi:10.1115/1.2930331

Labeas GN , Sunaric MM . Investigation on the static response and failure process of metallic open lattice cellular structures. Strain 2010;46(2):195–204 .

Li, B., Li, Z., Zhou, J., Ye, L., & Li, E. (2015). Damage localization in composite lattice truss core sandwich structures based on vibration characteristics. *Composite Structures*, *126*, 34–51. https://doi.org/10.1016/j.compstruct.2015.02.046

Liew, K. M., Peng, L. X., & Kitipornchai, S. (2009). Vibration analysis of corrugated Reissner-Mindlin plates using a mesh-free Galerkin method. International Journal of Mechanical Sciences, 51(9–10), 642–652.

Lou, J., Wu, L., Ma, L., Xiong, J., & Wang, B. (2014). Effects of local damage on vibration characteristics of composite pyramidal truss core sandwich structure. *Composites Part B: Engineering*, *62*, 73–87. https://doi.org/10.1016/j.compositesb.2014.02.012

Mines, R. A. W., Tsopanos, S., Shen, Y., Hasan, R., and McKown, S. T. (2013) 'Drop weight impact behaviour of sandwich panels with metallic micro lattice cores', International Journal of Impact Engineering, Vol. 60, pp. 120-132.

Mun, J., B.-G. Yun, J. Ju, and B.-M. Chang 2015. Indirect additive manufacturing based casting of a periodic 3d cellular metal{flow simulation of molten aluminum alloy. *Journal of Manufacturing Processes*, 17:28{40.

Ozdemir Z, Hernandez-nava E, Tyas A, et al. International Journal of Impact Engineering Energy absorption in lattice structures in dynamics : Experiments. *Int J Impact Eng*. 2016;89:49-61. doi:10.1016/j.ijimpeng.2015.10.007

Pietro Larizza, in Micromanufacturing Engineering and Technology (Second Edition), 2015

Queheillalt, D. T. and H. N. Wadley 2005. Cellular metal lattices with hollow trusses. Acta Materialia, 53(2):303{313.

Reddy, J. R., An Introduction to the Finite Element Method, McGraw-Hill, 2006.

Russel, R.C. (2013) Computer Finite Element Simulation In Mechanical Design. Master thesis. Retrieved from https://etd.library.vanderbilt.edu/available/etd-11182013 205832/unrestricted/Ryan_Russell.pdf

Salehian A, Inman DJ . Dynamic analysis of a lattice structure by homogenization: experimental validation. J Sound Vib 2008;316(1–5):180–97 .

Singh Rajawat, A., Sharma, A. K., & Gehlot, P. (2018). Free vibration analysis of Stiffened Laminated Plate using FEM. Materials Today: Proceedings, 5(2), 5313–5321.

Suard, M. 2015. Characterization and optimization of lattice structures made by Electron Beam Melting. PhD thesis, Univ. Grenoble Alpes.

S. R. Johnston, M. Reed, H. V. Wang and D. W. Rosen, "Analysis of mesostrucure unit cells comprised of octet-truss structures," in Proceedings of the Seventeenth Solid Freeform Fabrication Symposium, Austin, Texas, 2006, pp.

Syam, W. P., Jianwei, W., Zhao, B., Maskery, I., Elmadih, W., & Leach, R. (2018). Design and analysis of strut-based lattice structures for vibration isolation. Precision Engineering, 52, 494-506.

Vayre, B., F. Vignat, and F. Villeneuve 2012b. Metallic additive manufacturing: state-of-the-art review and prospects. Mechanics & Industry, 13(02):89{96.

Vannutelli, R., & Vannutelli, R. (2017). Mechanical Behavior of 3D Printed Lattice Structured Materials by, (December).

Vaz, J. da C., & de Lima Junior, J. J. (2014). Vibration analysis of Euler-Bernoulli beams in multiple steps and different shapes of cross section. Journal of Vibration and Control, 22(1), 193–204.

Vishnu, K.V., Bk, A., & Ks, A. (2015). Vibration Analysis: A Literature Review. IOSR Journal of Electronics and Communication Engineering Ver. II, 10(5), 2278-2834.

Wadley, H. N. 2002. Cellular metals manufacturing. Advanced Engineering Materials, 4(10):726{733.

Wang, X. , in Vehicle Noise and Vibration Refinement, 2010

Winter, R. E., Cotton, M., Harris, E. J., Maw, J. R., Chapman, D. J., Eakins, D. E., and McShane, G. (2014) 'Plate-impact loading of cellular structures formed by selective laser melting', Modelling and Simulation in Materials Science and Engineering, Vol. 22 No. 2, pp. 025021.

Yang, L., Cormier, D., West, H., Harrysson, O., & Knowlson, K. (2012). Non-stochastic Ti-6Al-4V foam structures with negative Poisson's ratio. *Materials Science and Engineering A*, *558*, 579–585. https://doi.org/10.1016/j.msea.2012.08.053

LIST OF APPENDICES

APPENDIX A

Sample of Calculation

1. **Stiffness, *k***

$$f = kx$$

$$k = \frac{f}{x}$$

$$k = \frac{10.00}{3.152 \text{ x } 10^{-4}}$$

k = 31.70 x 10^{3} N/m

APPENDIX B

Project Planning and Execution

Gant Chart

All the activities and planning for PSM 1 and PSM 2 is illustrated in Table below.

PROJECT PLANNING FOR PSM 1														
WEEK / **ACTIVITES**	**1**	**2**	**3**	**4**	**5**	**6**	**7**	**8**	**9**	**10**	**11**	**12**	**13**	**14**
Research Title Briefing								MID SEMESTER BREAK						
Literature Review														
Design of Lattice Structure														
Vibration Characteristic Using FEA														
Data Analysis														
Report Writing														
Report Submission														
PSM 1 Seminar														

PROJECT PLANNING FOR PSM 2															
WEEK / ACTIVITES	1	2	3	4	5	6	7	8	9	10	11	12	13	14	15
Vibration Characteristic Using FEA										MID SEMESTER BREAK					
Static Deflection Analysis Using FEA															
Conduct Modal Testing Experimentally															
Data Analysis															
Report Writing															
Report Submission															
PSM 2 Seminar															

APPENDIX C1

List of apparatus for conducting modal analysis experiment

Impact Hammer

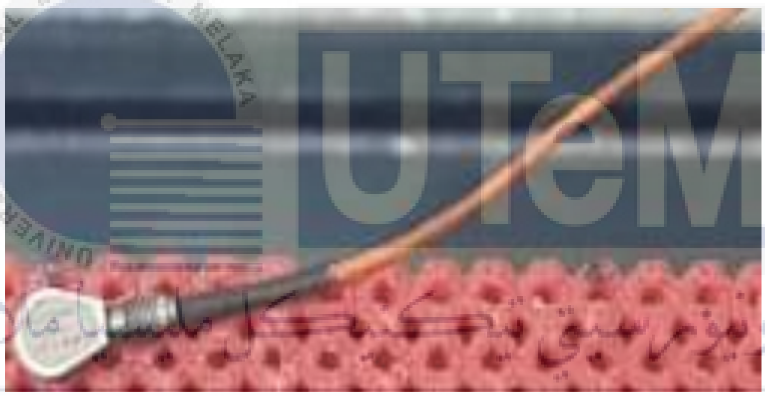

Accelerometer

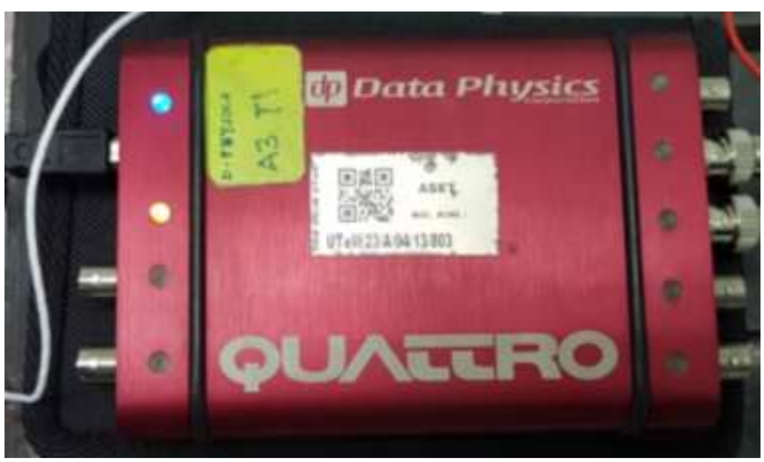

Data physic/Analyzer

Spanner

APPENDIX C2

Data materials

Overview of materials for Acrylonitrile Butadiene Styrene (ABS), Extruded

Categories: Polymer; Thermoplastic; ABS Polymer; Acrylonitrile Butadiene Styrene (ABS), Extruded

Material Notes: This property data is a summary of similar materials in the MatWeb database for the category "Acrylonitrile Butadiene Styrene (ABS), Extruded". Each property range of values reported is minimum and maximum values of appropriate MatWeb entries. The comments report the average value, and number of data points used to calculate the average. The values are not necessarily typical of any specific grade, especially less common values and those that can be most affected by additives or processing methods.

Vendors: **Click here to view all available suppliers for this material.**

Please click here if you are a supplier and would like information on how to add your listing to this material.

Physical Properties	Metric	English	Comments
Density	1.01 - 1.20 g/cc	0.0365 - 0.0434 lb/in^3	Average value: 1.05 g/cc Grade Count:120
Water Absorption	0.250 - 1.00 %	0.250 - 1.00 %	Average value: 0.448 % Grade Count:24
Moisture Absorption at Equilibrium	0.000 - 0.210 %	0.000 - 0.210 %	Average value: 0.180 % Grade Count:9
Water Absorption at Saturation	0.300 - 1.03 %	0.300 - 1.03 %	Average value: 0.796 % Grade Count:5
Maximum Moisture Content	0.0100 - 0.150	0.0100 - 0.150	Average value: 0.0256 Grade Count:9
Linear Mold Shrinkage	0.00200 - 0.00800 cm/cm	0.00200 - 0.00800 in/in	Average value: 0.00533 cm/cm Grade Count:79
Linear Mold Shrinkage, Transverse	0.00300 - 0.00800 cm/cm	0.00300 - 0.00800 in/in	Average value: 0.00591 cm/cm Grade Count:6
Melt Flow	0.100 - 35.0 g/10 min	0.100 - 35.0 g/10 min	Average value: 5.00 g/10 min Grade Count:120

Mechanical Properties	Metric	English	Comments
Hardness, Rockwell R	68.0 - 113	68.0 - 113	Average value: 101 Grade Count:63
Ball Indentation Hardness	65.0 - 110 MPa	9430 - 16000 psi	Average value: 93.2 MPa Grade Count:11
Tensile Strength, Ultimate	22.1 - 49.0 MPa	3210 - 7110 psi	Average value: 36.4 MPa Grade Count:31
Tensile Strength, Yield	13.0 - 65.0 MPa	1890 - 9430 psi	Average value: 40.5 MPa Grade Count:117
	22.1 - 59.3 MPa @Temperature -10.0 - 71.0 °C	3210 - 8600 psi @Temperature -0.400 - 160 °F	Average value: 40.7 MPa Grade Count:1
Elongation at Break	3.00 - 150 %	3.00 - 150 %	Average value: 34.2 % Grade Count:71
Elongation at Yield	0.620 - 30.0 %	0.620 - 30.0 %	Average value: 5.57 % Grade Count:49
Modulus of Elasticity	1.00 - 2.65 GPa	145 - 384 ksi	Average value: 2.07 GPa Grade Count:57
	1.50 - 2.60 GPa @Temperature 18.0 - 71.0 °C	218 - 377 ksi @Temperature -0.400 - 160 °F	Average value: 2.05 GPa Grade Count:1
Flexural Yield Strength	0.379 - 593 MPa	55.0 - 86000 psi	Average value: 69.2 MPa Grade Count:78
	49.6 - 113.8 MPa @Temperature -40.0 - 71.0 °C	7190 - 16510 psi @Temperature -40.0 - 160 °F	Average value: 81.7 MPa Grade Count:1
Flexural Modulus	0.200 - 5.50 GPa	29.0 - 798 ksi	Average value: 2.20 GPa Grade Count:105
	1.90 - 2.80 GPa @Temperature -40.0 - 71.0 °C	276 - 406 ksi @Temperature -40.0 - 160 °F	Average value: 2.35 GPa Grade Count:1
Izod Impact, Notched	0.380 - 10.3 J/cm	0.712 - 19.3 ft-lb/in	Average value: 3.22 J/cm Grade Count:88
	0.450 - 4.00425 J/cm @Temperature -40.0 - 0.000 °C	0.843 - 7.50160 ft-lb/in @Temperature -40.0 - 32.0 °F	Average value: 1.34 J/cm Grade Count:21
	0.480 - 4.00 J/cm @Temperature -40.0 - 0.000 °C	0.899 - 7.49 ft-lb/in @Temperature -40.0 - 32.0 °F	Average value: 1.34 J/cm Grade Count:12
	0.480 - 4.00 J/cm @Thickness 3.17 - 6.40 mm	0.899 - 7.49 ft-lb/in @Thickness 0.125 - 0.252 in	Average value: 1.34 J/cm Grade Count:12
Izod Impact, Unnotched	1.07873 - 1.66713 J/cm @Temperature -20.0 - -20.0 °C	2.02091 - 3.12322 ft-lb/in @Temperature -4.00 - -4.00 °F	Average value: 1.37 J/cm Grade Count:2
	1.07873 - 1.66713 J/cm @Thickness 3.20 - 6.40 mm	2.02091 - 3.12322 ft-lb/in @Thickness 0.126 - 0.252 in	Average value: 1.37 J/cm Grade Count:2
Izod Impact, Notched (ISO)	8.00 - 42.0 kJ/m^2	3.81 - 20.0 ft-lb/in^2	Average value: 26.4 kJ/m^2 Grade Count:24
	7.00 - 22.0 kJ/m^2 @Temperature -30.0 - -20.0 °C	3.33 - 10.5 ft-lb/in^2 @Temperature -22.0 - -4.00 °F	Average value: 13.0 kJ/m^2 Grade Count:15
	7.00 - 7.00 kJ/m^2 @Temperature -40.0 - -40.0 °C	3.33 - 3.33 ft-lb/in^2 @Temperature -40.0 - -40.0 °F	Average value: 13.0 kJ/m^2 Grade Count:1
	7.00 - 7.00 kJ/m^2 @Thickness 4.00 - 4.00 mm	3.33 - 3.33 ft-lb/in^2 @Thickness 0.157 - 0.157 in	Average value: 13.0 kJ/m^2 Grade Count:1
Charpy Impact Unnotched	11.0 J/cm^2 - NB	52.4 ft-lb/in^2 - NB	Average value: 15.4 J/cm^2 Grade Count:19
	1.00 J/cm^2 - NB @Temperature -40.0 - -30.0 °C	4.76 ft-lb/in^2 - NB @Temperature -40.0 - -22.0 °F	Average value: 8.56 J/cm^2 Grade Count:20
Charpy Impact, Notched	0.700 - 5.00 J/cm^2	3.33 - 23.8 ft-lb/in^2	Average value: 2.46 J/cm^2 Grade Count:29
	0.500 - 2.50 J/cm^2 @Temperature -30.0 - -20.0 °C	2.38 - 11.9 ft-lb/in^2 @Temperature -22.0 - -4.00 °F	Average value: 1.43 J/cm^2 Grade Count:18
Dart Drop, Total Energy	24.4 - 50.2 J	18.0 - 37.0 ft-lb	Average value: 31.9 J Grade Count:5
Falling Dart Impact	19.0 - 569 J	14.0 - 420 ft-lb	Average value: 185 J Grade Count:3
Instrumented Impact Total Energy	14.0 - 47.5 J	10.3 - 35.0 ft-lb	Average value: 24.1 J Grade Count:4
Instrumented Impact Energy at Peak	11.0 - 33.9 J	8.11 - 25.0 ft-lb	Average value: 18.8 J Grade Count:3

Titanium Ti-6Al-4V (Grade 5), Annealed Bar

Categories: Metal; Nonferrous Metal; Titanium Alloy; Alpha/Beta Titanium Alloy

Material Notes:

Information provided by Allvac and the references. Annealing Temperature 700-785°C. Alpha-Beta Alloy

Applications: Blades, discs, rings, airframe, fasteners, components. Vessels, cases, hubs, forgings. Biomedical implants.

Biocompatibility: Excellent, especially when direct contact with tissue or bone is required. Ti-6Al-4V's poor shear strength makes it undesirable for bone screws or plates. It also has poor surface wear properties and tends to seize when in sliding contact with itself and other metals. Surface treatments such as nitriding and oxidizing can improve the surface wear properties.

4 other heat treatments of this alloy are listed in MatWeb.

Key Words: Ti-6-4; UNS R56400; ASTM Grade 5 titanium; Ti6Al4V, Ti64, biomaterials, biomedical implants, biocompatibility

Vendors:

Physical Properties	Metric	English	Comments
Density	4.43 g/cc	0.160 lb/in³	

Mechanical Properties	Metric	English	Comments
Hardness, Brinell	334	334	Estimated from Rockwell C.
Hardness, Knoop	363	363	Estimated from Rockwell C.
Hardness, Rockwell C	36	36	
Hardness, Vickers	349	349	Estimated from Rockwell C.
Tensile Strength, Ultimate	900 MPa	131000 psi	
Tensile Strength, Yield	830 MPa	120000 psi	
Elongation at Break	10 %	10 %	
Reduction of Area	33 %	33 %	
Modulus of Elasticity	114 GPa	16500 ksi	Average of tension and compression
Compressive Yield Strength	860 MPa	125000 psi	
Poissons Ratio	0.33	0.33	
Fatigue Strength	510 MPa @# of Cycles 1.00e+7	74000 psi @# of Cycles 1.00e+7	smooth
Shear Modulus	44.0 GPa	6380 ksi	

Electrical Properties	Metric	English	Comments
Electrical Resistivity	0.000178 ohm-cm	0.000178 ohm-cm	
Magnetic Permeability	1.00005	1.00005	at 1.6 kA/m
Magnetic Susceptibility	0.0000033	0.0000033	cgs/g

Thermal Properties	Metric	English	Comments
CTE, linear	8.60 µm/m-°C @Temperature 20.0 - 100 °C	4.78 µin/in-°F @Temperature 68.0 - 212 °F	
	9.20 µm/m-°C @Temperature 20.0 - 315 °C	5.11 µin/in-°F @Temperature 68.0 - 599 °F	average
	9.70 µm/m-°C @Temperature 20.0 - 650 °C	5.39 µin/in-°F @Temperature 68.0 - 1200 °F	average
Specific Heat Capacity	0.5263 J/g-°C	0.1258 BTU/lb-°F	
Thermal Conductivity	6.70 W/m-K	46.5 BTU-in/hr-ft²-°F	
Melting Point	1604 - 1660 °C	2919 - 3020 °F	
Solidus	1604 °C	2919 °F	
Liquidus	1660 °C	3020 °F	
Beta Transus	980 °C	1800 °F	

Component Elements Properties	Metric	English	Comments
Aluminum, Al	5.5 - 6.75 %	5.5 - 6.75 %	
Carbon, C	<= 0.080 %	<= 0.080 %	
Hydrogen, H	<= 0.015 %	<= 0.015 %	
Iron, Fe	<= 0.40 %	<= 0.40 %	
Nitrogen, N	<= 0.030 %	<= 0.030 %	
Other, each	<= 0.050 %	<= 0.050 %	
Other, total	<= 0.30 %	<= 0.30 %	

316 Stainless Steel, annealed bar

Categories:	Metal; Ferrous Metal; Stainless Steel; T 300 Series Stainless Steel
Material Notes:	Molybdenum content increases resistance to marine environments. High creep strength at elevated temperatures and good heat resistance. Biocompatible. Fabrication characteristics similar to Types 302 and 304. **Applications:** food and pharmaceutical processing equipment, marine exterior trim, surgical implants, and industrial equipment that handles the corrosive process chemicals used to produce inks, rayons, photographic chemicals, paper, textiles, bleaches, and rubber. **Corrosion Resistance:** better corrosion resistance than 302 and 304; resists sodium and calcium brines; hypochlorite solutions, phosphoric acid; and the sulfite liquors and sulfurous acids used in the paper pulp industry.
Key Words:	UNS S31600, SS316, 316SS, AISI 316, DIN 1.4401, DIN 1.4408, DIN X5CrNiMo17122, TGL 39672 X5CrNiMo1911, TGL 7143X5CrNiMo1811, ISO 2604-1 F62, ISO 2604-2 TS60, ISO 2604-2 TS61, ISO 2604-4 P60, ISO 2604-4 P61, ISO 4954 X5CrNiMo17122E, ISO 683/13 20, ISO 683/13 20a, ISO 6931 X5CrNiMo17122, JIS SUS 316
Vendors:	**Click here to view all available suppliers for this material.** Please click here if you are a supplier and would like information on how to add your listing to this material.

Physical Properties	Metric	English	Comments
Density	8.00 g/cc	0.289 lb/in³	

Mechanical Properties	Metric	English	Comments
Hardness, Brinell	149	149	
Hardness, Knoop	169	169	Converted from Brinell
Hardness, Rockwell B	80	80	
Hardness, Vickers	155	155	Converted from Brinell
Tensile Strength, Ultimate	550 MPa	79800 psi	
Tensile Strength, Yield	240 MPa	34800 psi	
Elongation at Break	60 %	60 %	in 50 mm
Modulus of Elasticity	193 GPa	28000 ksi	
Izod Impact	129 J	95.1 ft-lb	
Charpy Impact	105 J	77.4 ft-lb	V-notch

Electrical Properties	Metric	English	Comments
Electrical Resistivity	0.0000740 ohm-cm	0.0000740 ohm-cm	at 20°C
Magnetic Permeability	1.008	1.008	at RT

Thermal Properties	Metric	English	Comments
CTE, linear	16.0 µm/m-°C @Temperature 0.000 - 100 °C	8.89 µin/in-°F @Temperature 32.0 - 212 °F	
	16.2 µm/m-°C @Temperature 0.000 - 315 °C	9.00 µin/in-°F @Temperature 32.0 - 599 °F	
	17.5 µm/m-°C @Temperature 0.000 - 540 °C	9.72 µin/in-°F @Temperature 32.0 - 1004 °F	
Specific Heat Capacity	0.500 J/g-°C @Temperature 0.000 - 100 °C	0.120 BTU/lb-°F @Temperature 32.0 - 212 °F	
Thermal Conductivity	16.3 W/m-K @Temperature 100 °C	113 BTU-in/hr-ft²-°F @Temperature 212 °F	
Melting Point	1370 - 1400 °C	2500 - 2550 °F	
Solidus	1370 °C	2500 °F	
Liquidus	1400 °C	2550 °F	
Maximum Service Temperature, Air	870 °C	1600 °F	Intermittent
	925 °C	1700 °F	Continuous Service

Component Elements Properties	Metric	English	Comments
Carbon, C	<= 0.080 %	<= 0.080 %	
Chromium, Cr	16 - 18 %	16 - 18 %	
Iron, Fe	61.8 - 72 %	61.8 - 72 %	As Remainder
Manganese, Mn	<= 2.0 %	<= 2.0 %	
Molybdenum, Mo	2.0 - 3.0 %	2.0 - 3.0 %	
Nickel, Ni	10 - 14 %	10 - 14 %	
Phosphorous, P	<= 0.045 %	<= 0.045 %	
Silicon, Si	<= 1.0 %	<= 1.0 %	
Sulfur, S	<= 0.030 %	<= 0.030 %	

References for this datasheet.

Appendix C3

Analysis of results for experiments

Strut Ø (mm)	1.4	1.6
FRF	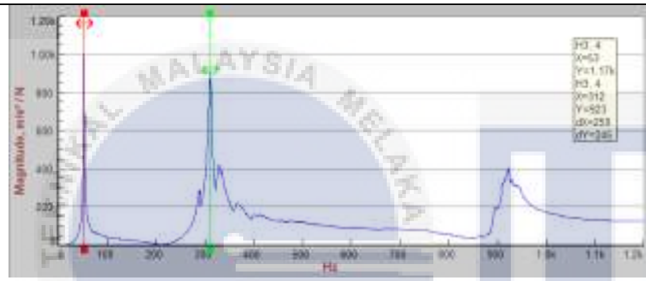	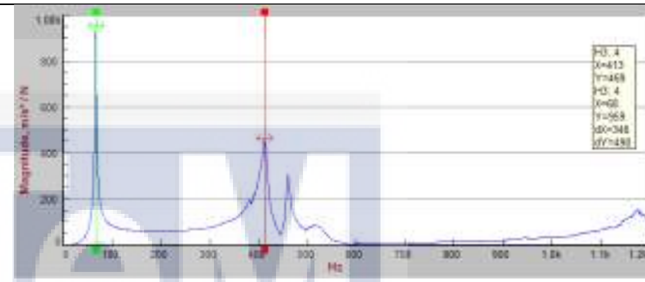
Bode Plot	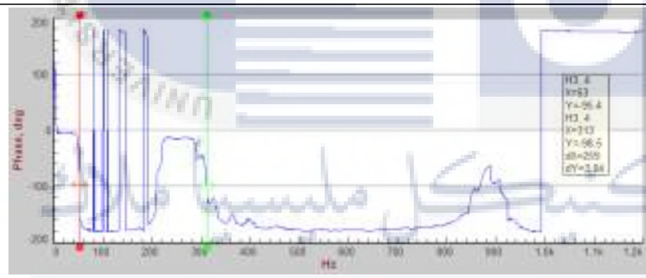	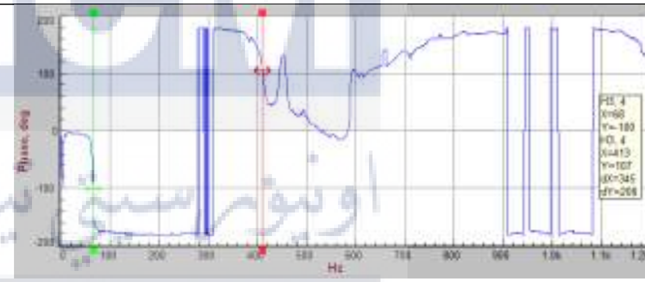
Coherence	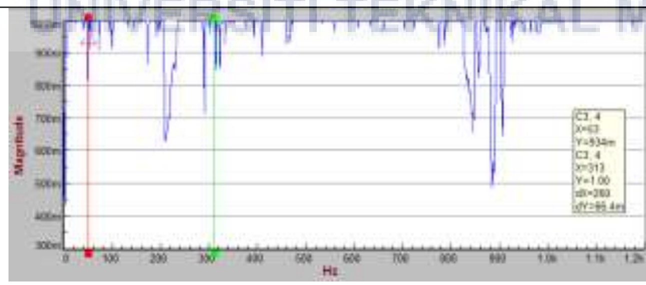	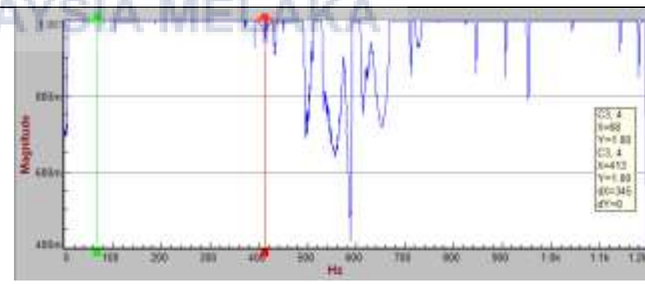

Strut Ø (mm)	1.8	Solid ABS
FRF	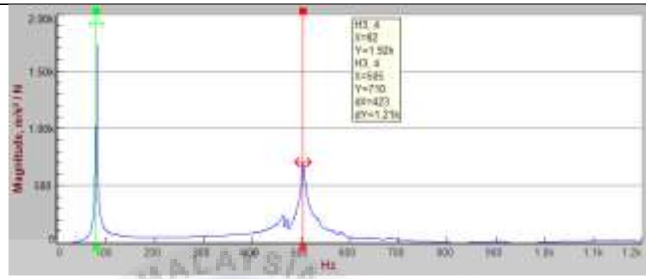	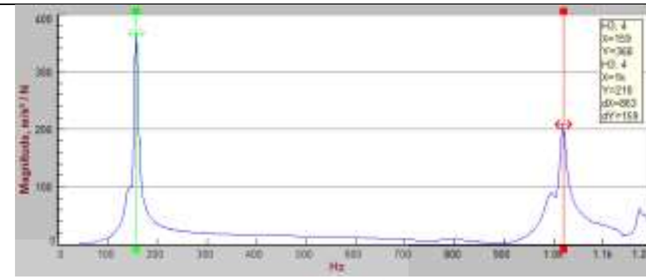
Bode Plot	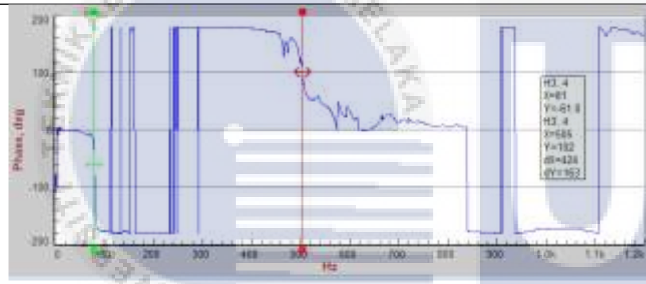	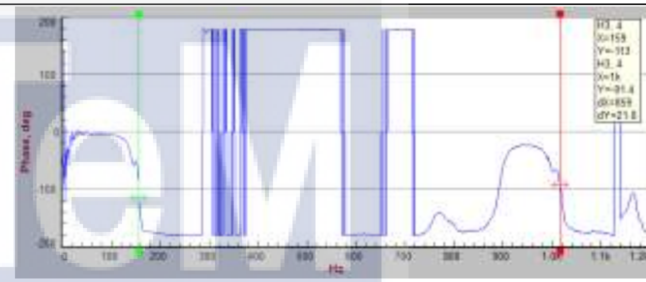
Coherence